The Astronomical Journal, 143:121 (18pp), 2012 May doi:10.1088/0004-6256/143/5/121

ULTRAVIOLET PROPERTIES OF GALACTIC GLOBULAR CLUSTERS WITH *GALEX*. I. THE COLOR–MAGNITUDE DIAGRAMS*

Ricardo P. Schiavon[1], Emanuele Dalessandro[2], Sangmo T. Sohn[3], Robert T. Rood[4,10], Robert W. O'Connell[4], Francesco R. Ferraro[2], Barbara Lanzoni[2], Giacomo Beccari[5], Soo-Chang Rey[6], Jaehyon Rhee[1,7], R. Michael Rich[8], Suk-Jin Yoon[9], and Young-Wook Lee[9]

[1] Gemini Observatory, 670 N. A'Ohoku Place, Hilo, HI 96720, USA; rschiavon@gemini.edu
[2] Dipartimento di Astronomia, Università degli Studi di Bologna, via Ranzani 1, I-40127 Bologna, Italy; emanuele.dalessandr2@unibo.it, francesco.ferraro3@unibo.it, barbara.lanzoni@unibo.it
[3] Space Telescope Science Institute, 3700 San Matin Dr., Baltimore, MD 21218, USA; tsohn@stsci.edu
[4] Astronomy Department, University of Virginia, P.O. Box 400325, Charlottesville, VA 22904, USA; rwo@virginia.edu
[5] ESO—European Southern Observatory, Karl-Swarzschild Str. 2, D-85748 Garching bei Munchen, Germany; gbeccari@eso.org
[6] Department of Astronomy and Space Science, Chungnam National University, Daejeon 305-764, Republic of Korea; screy@cnu.ac.kr
[7] Department of Physics, Purdue University, 525 Northwestern Avenue, West Lafayette, IN 47907, USA; jrhee@gemini.edu
[8] Department of Physics and Astronomy, University of California, Los Angeles, USA; rmr@astro.ucla.edu
[9] Center for Galaxy Evolution Research and Department of Astronomy, Yonsei University, Seoul 120-749, Republic of Korea; sjyoon@galaxy.yonsei.ac.kr, ywlee2@yonsei.ac.kr
Received 2011 October 3; accepted 2012 January 22; published 2012 April 16

ABSTRACT

We present *Galaxy Evolution Explorer* (*GALEX*) data for 44 Galactic globular clusters (GCs) obtained during three *GALEX* observing cycles between 2004 and 2008. This is the largest homogeneous data set on the UV photometric properties of Galactic GCs ever collected. The sample selection and photometric analysis are discussed, and color–magnitude diagrams (CMDs) are presented. The blue and intermediate-blue horizontal branch is the dominant feature of the UV CMDs of old Galactic GCs. Our sample is large enough to display the remarkable variety of horizontal branch shapes found in old stellar populations. Other stellar types that are obviously detected are blue stragglers and post-core-He burning stars. The main features of UV CMDs of Galactic GCs are briefly discussed. We establish the locus of post-core-He burning stars in the UV CMD and present a catalog of candidate asymptotic giant branch (AGB), AGB-manqué, post early-AGB, and post-AGB stars within our cluster sample.

Key words: globular clusters: general – Hertzsprung-Russell and C-M diagrams – stars: evolution

1. INTRODUCTION

It is fair to say that the last frontier of our growing understanding of the physics of old stellar populations resides in the ultraviolet (UV). The behavior of old stellar populations in the UV has puzzled astronomers for almost four decades now, and in spite of major recent progress, there are still important gaps in our understanding of the nature of the stars that dominate the integrated light of old stellar populations in the UV—particularly the far-UV (FUV, e.g., Ferraro et al. 1998; O'Connell 1999; Moehler 2001; Catelan 2009). These include the extreme horizontal branch (EHB) and Blue-Hook (BHk) stars, at the hot and visually faint end of the horizontal branch (HB), and the short-lived but more luminous supra-HB and post-asymptotic-giant-branch (PAGB) stars. Another population whose nature is still not entirely well understood is that of blue straggler stars, which at the characteristic ages of Galactic globular clusters (GCs) are not hot enough to contribute substantially to the integrated FUV light, but are an important source of near-UV light (NUV, e.g., Ferraro et al. 2001, 2003), and are in some cases detectable in integrated light longward of 3400 Å (e.g., Trager et al. 2005; Schiavon 2007).

The UV properties of old stellar populations have been a subject of intense scrutiny ever since the discovery of the "UV-upturn" of early-type galaxies (Code 1969). While it has become clear in the past decade or so that EHBs are responsible for most of the "excess" UV emission observed in old stellar populations (e.g., Greggio & Renzini 1990, 1999; Dorman et al. 1995; O'Connell 1999; Brown et al. 2001), our understanding of the physics underlying the structure and evolution of such stars is still plagued by theoretical uncertainties. Undeniably, uncertainties are partly due to the absence of an accurate, comprehensive, statistically representative, homogeneous data set presenting the colors and magnitudes of the stars responsible for the UV emission in Galactic GCs—in spite of painstaking observational efforts by a number of groups (for reviews see, e.g., O'Connell 1999; Moehler 2001). A database of that kind would also have important applications for studies of extragalactic stellar populations, as it could be used to unveil correlations between features in the color–magnitude diagrams (CMDs) of stellar populations and their integrated properties. Such correlations can help understand the nature of distant systems, for which only integrated properties are available. In particular, direct comparisons between integrated UV properties of Galactic and extragalactic GCs (e.g., Sohn et al. 2006; Rey et al. 2007, 2009) can lend insights on the stellar population content of those systems (Dalessandro et al. 2012, hereafter Paper II).

With this motivation in mind, we decided to use the *Galaxy Evolution Explorer* (*GALEX*) to undertake the largest ever systematic and homogeneous census of the UV properties of Galactic GCs. Data were collected for 44 clusters in three *GALEX* cycles, from which UV CMDs and integrated colors were obtained. This paper discusses the sample selection and the photometric analysis of the data. Some of the data have been used in combination with *Hubble Space Telescope* (*HST*)

* The authors dedicate this paper to the memory of co-author Bob Rood, a pioneer in the theory of the evolution of low-mass stars, and a friend, who sadly passed away on 2011 November 2.
[10] Deceased.

Figure 1. False color picture of one of the fields targeted in our survey. North is up, east is left, and the vertical size is ∼37′. There is a population of very blue stars covering the entire field, with a higher density toward the SE. These are main-sequence stars belonging to the Small Magellanic Cloud. The cluster located on the upper right of the picture is NGC 362. Blue horizontal branch stars in NGC 362 appear as white colored objects within a few arcminutes from the cluster center.

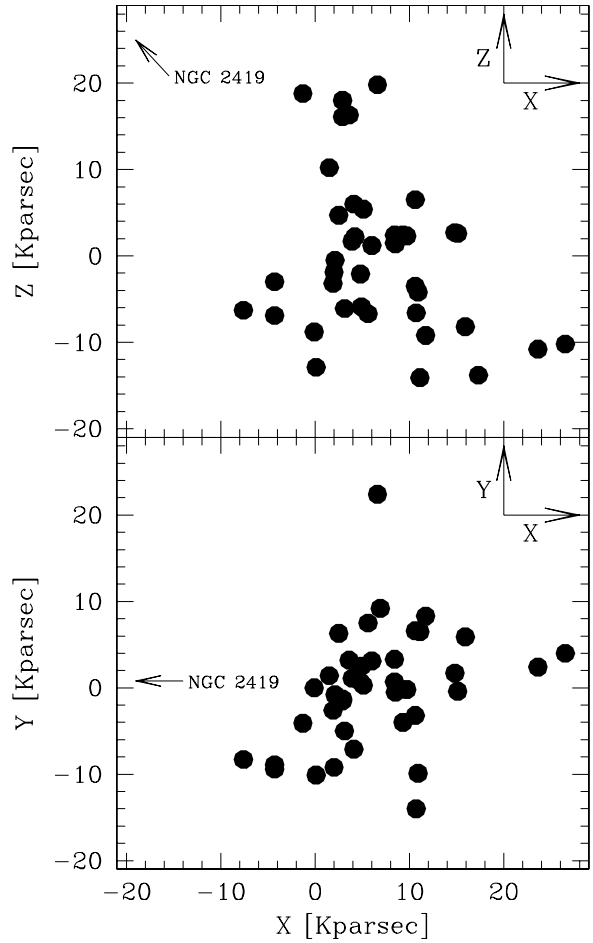

Figure 2. Spatial distribution of Galactic GCs in our sample. Note that NGC 2419, located at a distance of 80 kpc from the Galactic center, is outside the plot limits.

and ground-based observations for multi-band photometric investigations of the stellar populations of NGC 1904 (Lanzoni et al. 2007) and M 2 (Dalessandro et al. 2009), from the innermost regions to the extreme outskirts of those clusters. Paper II describes the derivation of integrated magnitudes for this cluster sample and presents an analysis of correlations between integrated magnitudes and colors and global cluster properties. Paper III (R. T. Rood et al. 2012, in preparation) introduces a new classification scheme of the HBs of Galactic GCs, based on their UV morphologies.

This paper is laid out as follows. Section 2 describes the sample selection, observations, data reduction, and analysis. In Section 3 the CMDs are presented. A description of our new catalog of post-He-core-burning star candidates is presented in Section 4. Our conclusions are summarized in Section 5.

2. OBSERVATIONS AND DATA ANALYSIS

GALEX is a 50 cm orbiting UV telescope launched in 2003 April. *GALEX* has a circular field of view (FOV) of ∼1.°2 diameter and, in imaging mode, a dichroic beam splitter allows it to collect data in two simultaneous channels, in FUV and NUV bands, corresponding to $\lambda = 1350$–1780 and 1770–2730 Å ($\lambda_{\rm eff} = 1516$ and 2267 Å) and with a spatial resolution of ∼4.″5 and 5.″5, respectively. *GALEX* detectors consist of two stacks of three large format microplate channels and associated electronics inserted in sealed tubes. The NUV and FUV detectors differ mostly in terms of the photocathode material (CsI in the case of FUV and Cs_2Te in the case of NUV) and the windows (MgF_2 for FUV, fused silica for NUV). The *GALEX* detectors record lists of time-ordered photon positions and pulse heights, and these are pipeline processed on the ground for image reconstruction. The resulting images have pixel scales of 1.5 arcsec pixel^{-1} in both FUV and NUV. Both detectors can be damaged by high global and per/pixel count rates, which prevents targeting very (UV-) bright stars and the low Galactic latitude regions, due to their high UV background. For more details, see Morrissey et al. (2005), Morrissey et al. (2007), or the *GALEX* instrument overview at http://galexgi.gsfc.nasa.gov/docs/galex/Documents/MissionOverview.html.

2.1. Sample and Observations

The data presented in this paper were primarily collected under *GALEX* GI programs 056 and 099 (PI: R. Schiavon) in Cycles 1 and 4, respectively. The target selection was performed with an eye toward spanning a wide range in metallicity and HB morphology. Limitations, however, were imposed by target magnitudes and the safety of *GALEX*'s UV detectors, so that very distant, heavily extinguished, and low Galactic latitude clusters could not be included in the sample. As a result, a number of interesting clusters, particularly metal-rich ones at low Galactic latitudes, were not observed, because the high UV background in these regions could potentially harm the *GALEX* detectors. Clusters with very UV-bright stars within the *GALEX* FOV also could not be observed (most notably ω Cen and NGC 6752) and in some cases the pointing had to be

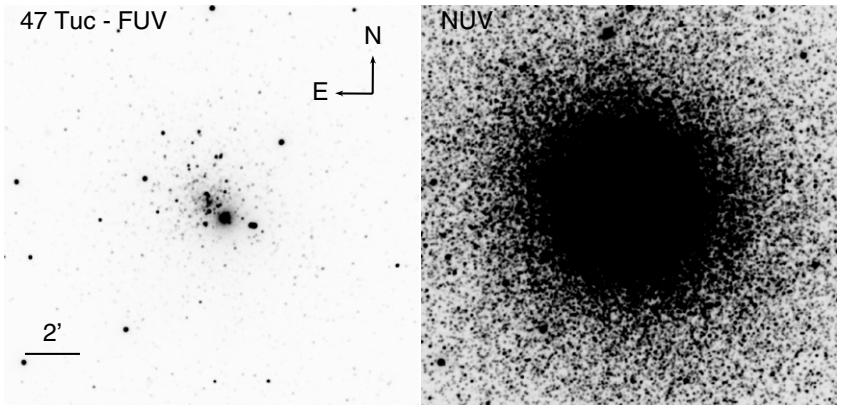

Figure 3. FUV and NUV images of 47 Tuc, the reddest cluster in our sample. Note the vast difference in the crowding of the two images, which renders NUV photometry impossible in the cluster core, at the spatial resolution of *GALEX*. The FUV light of the cluster is due to a few dozen sources, with roughly half of it being due to a single very bright star (47 Tuc BS; O'Connell et al. 1997). Photometry in the FUV is accurate even in the central cluster regions.

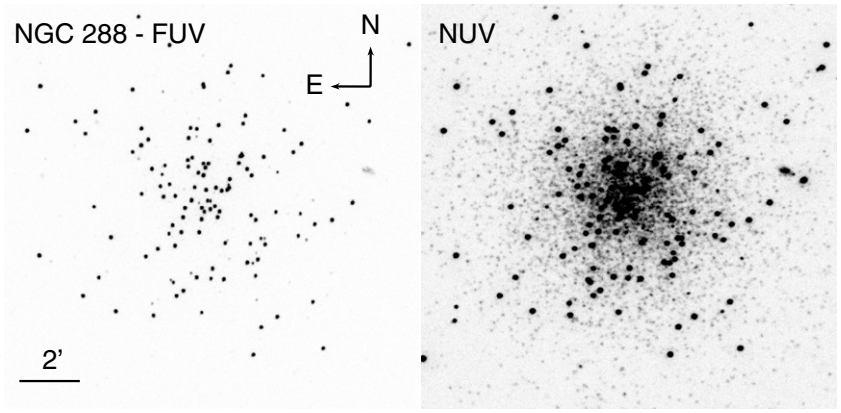

Figure 4. FUV and NUV images of NGC 288, with a lower overall surface brightness than 47 Tuc, yet with a larger population of FUV sources—though not large enough to present problems for FUV photometry in the central regions. In the NUV, crowding is much more important, yet photometry at the resolution of *GALEX* is still achievable, though with lower precision.

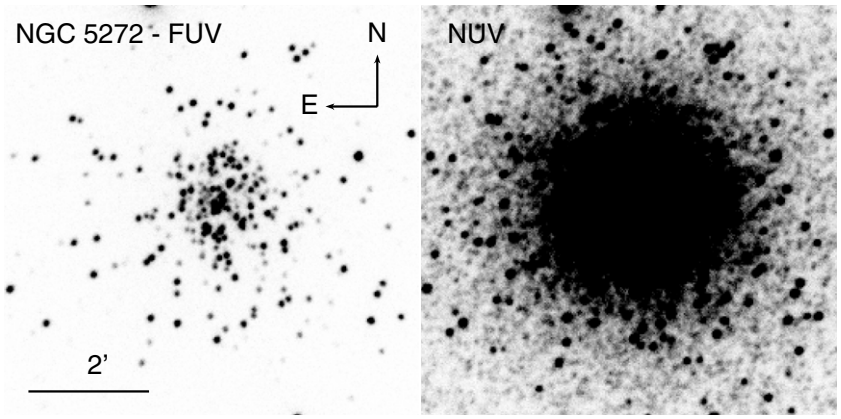

Figure 5. FUV and NUV images of NGC 5272. Note that stellar density is high enough that even FUV photometry is slightly more uncertain than in the cases of NGC 288 and 47 Tuc.

adjusted in order to exclude such stars from the FOV. The target list for Cycle 1 totaled 25 Galactic GCs and was composed primarily of clusters for which EHB stars could be detected in both FUV and NUV bands in a single *GALEX* orbit, with typical exposure times of 1500 s.

For Cycle 4, our strategy entailed deeper exposures on a smaller sample of 15 clusters, with a focus on expanding coverage toward higher metallicity and younger age, while including clusters of known extragalactic origin, such as Arp 2 and Terzan 8 (e.g., Law & Majewski 2010). We also took advantage of the relaxation of the UV-brightness constraints dictated by detector-safety considerations in order to obtain data for metal-rich Galactic GCs at relatively low Galactic latitude, such as NGC 6342 and NGC 6356. For the latter, as well as for very distant Galactic GCs (NGC 2419, Terzan 8, Arp 2, IC 4499) we originally had little hope of obtaining good quality CMDs,

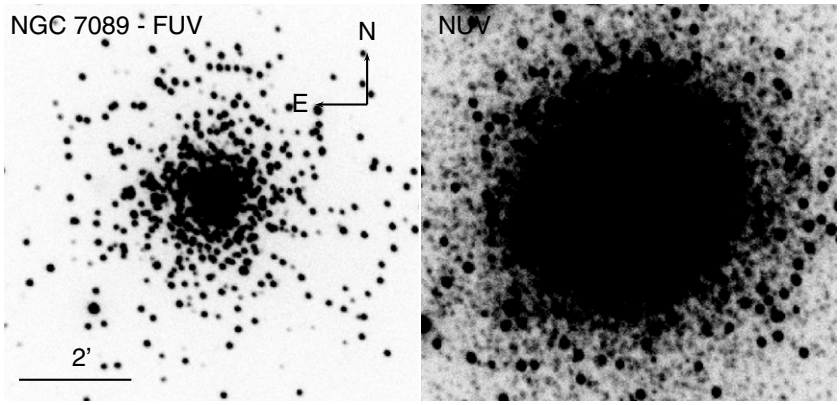

Figure 6. FUV and NUV images of NGC 7089, one of the densest clusters in our sample. In this extreme case, even FUV photometry is hampered in the core cluster regions.

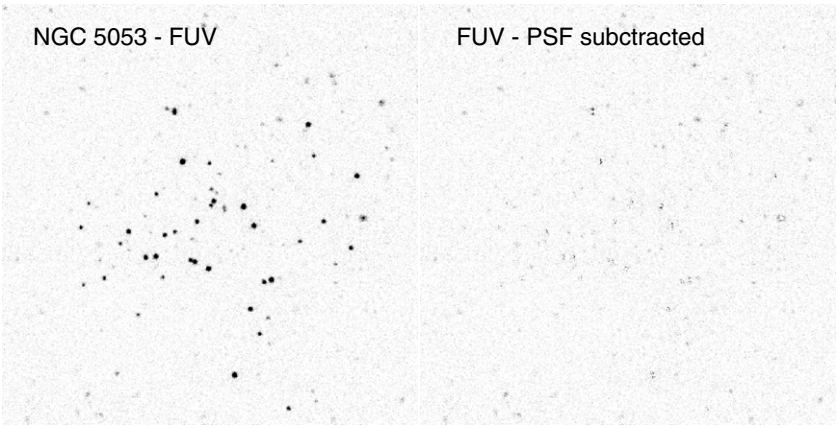

Figure 7. Quality of PSF modeling in a good case: NGC 5053 in the FUV. Due to low density, PSF residuals are negligible and good quality photometry is achieved for all cluster stars in the FUV.

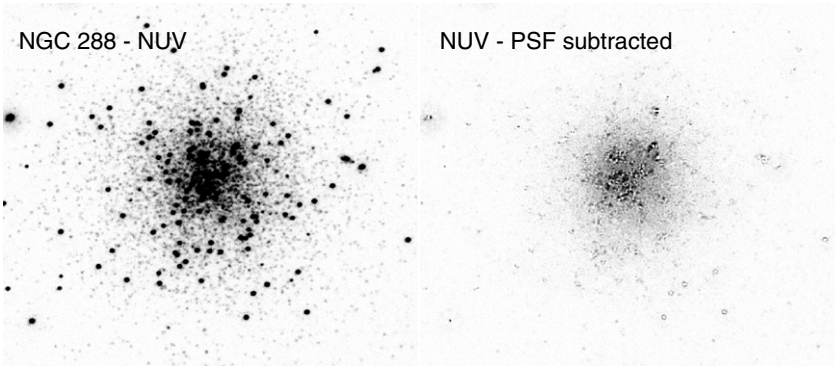

Figure 8. Quality of PSF modeling in a typical case: NGC 288 in the NUV. Crowding in the central regions is relatively high, at the resolution of *GALEX*, photometry is relatively inaccurate for stars within $\sim 0\farcm5$ from the cluster center. The PSF-subtracted image shows a diffuse residual, associated with the detection of NUV light from unresolved turnoff stars.

and just aimed at measuring reliable integrated colors (but see discussion in Section 3). For one cluster (NGC 6273) NUV data were not collected.

Finally, we further include data for six out of eight Galactic GCs from Cycle 3 GI program 075 (PI: S. T. Sohn), which aimed at measuring reliably UV fluxes of extreme HB stars in the program clusters to test the helium-rich hypothesis for the production of EHB stars (e.g., Lee et al. 2005). We plan to present the results of this analysis in a forthcoming paper (Paper IV; S. T. Sohn et al. 2012, in preparation). For the Cycle 3 program we selected clusters that exhibit extended HB blue tails in their optical CMDs.

As mentioned above, our original proposals for Cycles 1 and 4 requested between 1 and 2 orbits to be spent on each cluster, which would have resulted in maximum exposure times of approximately 3000 s on both bands for each target. However, our program benefited from the complexities of *GALEX* queue scheduling so that longer exposure times were achieved for some clusters—in some cases, such as that of NGC 2298, exposure times were an order of magnitude longer. Exposure times are also in general longer in the NUV than in the FUV, which is due to the several events of FUV detector shutoffs caused by overcurrents in the FUV detector. Repeated attempts of collecting FUV data led therefore to an accumulation of NUV

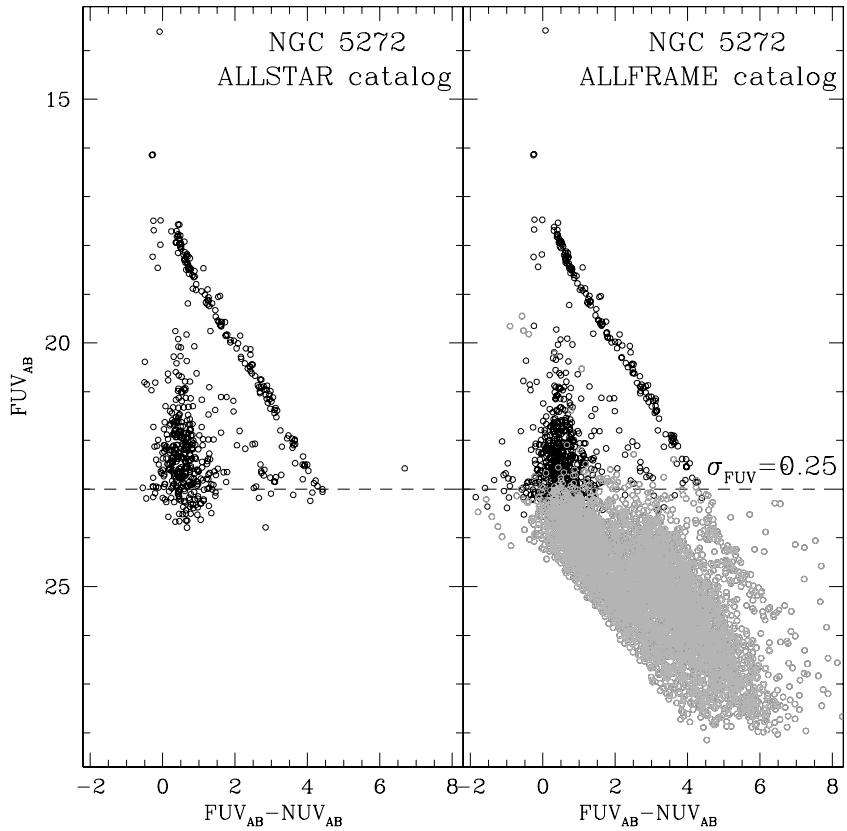

Figure 9. Results from tests aimed at assessing the depth of our photometry. The left panel shows the CMD based on `allstar`, while the right panel shows the CMD obtained by "force-finding" stars in FUV on the basis of their position in NUV by using `allframe`. The dashed horizontal line marks the limit corresponding to the photometric error $\sigma_{\rm FUV} = 0.25$.

exposures. In total, our program accrued 340 ks of open shutter time, or the equivalent of ∼226 *GALEX* orbits. A false color picture of the field containing one of our clusters (NGC 362) is shown in Figure 1. The spatial distribution of our cluster sample is displayed in Figure 2.

2.2. Photometry and Calibration

The quality and depth of our data are illustrated in Figures 3–6, where NUV and FUV images of a representative subset of the sample are displayed. Consistent gray scales were adopted when producing these images, to allow for a fair visual assessment of the various degrees of crowdedness of Galactic GCs, as seen on both *GALEX* bands. To the same end, image sizes are set such that the FOV is equal to ∼5 times the cluster's core radii. Displayed is one of the reddest clusters in our sample (47 Tuc) together with bluer clusters, spanning a range of stellar density, increasing from NGC 288 to NGC 5272, and NGC 7089. As a general rule, one can see that stellar density is significantly higher in the NUV than in the FUV. This is because, on one hand, the combination of higher sensitivity and longer exposure time makes NUV images a lot deeper than their FUV counterparts and, on the other hand, Galactic GC stars are predominantly brighter in NUV than in FUV. As a result, even at the relatively low resolution of *GALEX*, accurate FUV photometry can be obtained down to the cores of most clusters in our sample (47 Tuc and NGC 288 being two cases in point), getting progressively difficult at increasing cluster density, up to a limit where crowding becomes a problem in the cluster central regions (e.g., NGC 7089). Unlike the FUV, crowding in the NUV is a problem in the central regions of almost all clusters in our sample. The effect of crowding on our CMDs is discussed in Section 3.

The photometric analysis was performed on the background-subtracted intensity images output by the *GALEX* pipeline (Morrissey et al. 2007, hereafter M07). These are 3840 × 3840 pixel^2 images with a plate scale of 1.″5 pixel^{-1}, covering a circular area of 1.°2 in diameter, flat-field corrected and with the flux normalized by the effective area and exposure time. Photometry was performed by following standard procedures for point-spread function (PSF) modeling, using the crowded-field photometry package `DAOPHOTII` (Stetson 1987) for both FUV and NUV images. The first step consists of defining a number of bright stars across the FOV for PSF modeling. For that purpose, we performed a very shallow search for bright point sources with the `DAOPHOT` task `find` on each image. Magnitudes at this stage, before PSF modeling, were based on simple aperture photometry obtained using the task `photometry` with an aperture radius $r = 4.''5$. We then selected relatively isolated bright stars spread across the FOV, for PSF determination. We avoided stars in the very central and crowded regions.

The PSF model was typically based on 200 stars in NUV and 50 in FUV images. Quadratic spatial variations of the PSF model were considered. Once the PSF model was determined, we reran `find` and `photometry` with appropriate threshold levels (typically 3σ–6σ off the sky background) in order to generate a more complete and deeper list of target stars for photometry. Magnitudes were then obtained for this expanded list by performing PSF fits using the `allstar` routine. Tests were performed where PSF photometry was carried out replacing the PSFs derived in this analysis by the average PSFs supplied

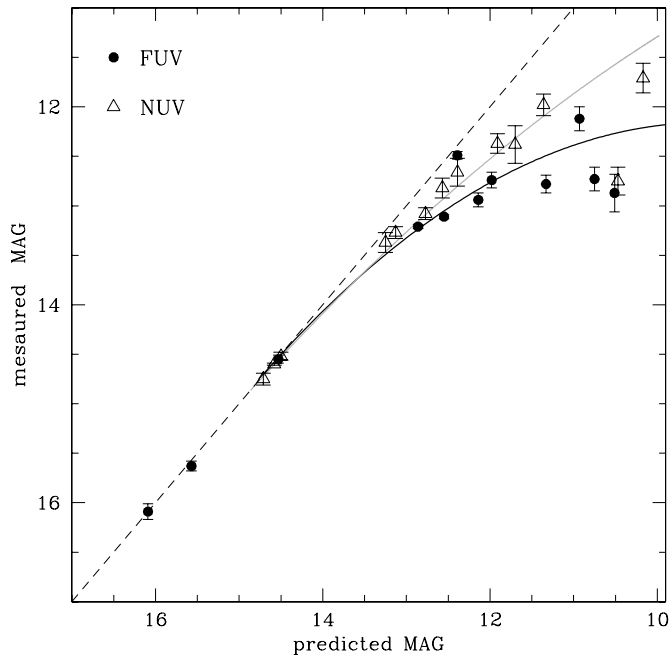

Figure 10. Results of tests for deviations from linearity in *GALEX* detectors. A comparison is shown between "predicted" and measured magnitudes for a number of standard stars from the CALSPEC database (see text). "Predicted" values are magnitudes obtained through synthetic photometry on CALSPEC spectra by M07, while measured values are aperture magnitudes by M07 (curves) and PSF magnitudes from this work (data points). Gray (black) curves and open (filled) symbols represent NUV (FUV) magnitudes. Saturation becomes important at 14.5 mag for both channels alike, but is more intense in the FUV channel for brighter sources. Our PSF photometry seems to be only slightly more affected than M07's aperture photometry, in the FUV channel only. Only a handful of stars in our entire sample are substantially affected by detector nonlinearity.

by the *GALEX* team.[11] No significant differences between these tests and the original photometry were found for a couple of clusters bracketing the full range of stellar densities and number of clean stars available for PSF determination.

Aperture corrections (typically ∼0.2 mag) were calculated on each image by using 15–20 isolated and bright stars, which were used to generate reliable curves of growth. Instrumental magnitudes were converted to the ABMAG photometric system, using the zero points provided by M07, as follows:

$$\mathrm{FUV} = -2.5\ \log(\mathrm{counts\ s^{-1}}) + 18.82 \quad (1)$$

$$\mathrm{NUV} = -2.5\ \log(\mathrm{counts\ s^{-1}}) + 20.08. \quad (2)$$

To illustrate the quality of the PSF modeling, we show in Figures 7 and 8 typical residuals from PSF subtraction in FUV and NUV images, respectively. Visual inspection shows that in low density areas, such as the FUV image of NGC 5053 in Figure 7 and the NUV image of NGC 288 outside the cluster core in Figure 8, stellar brightness profiles are properly reproduced by the PSF models used. In contrast, residuals are much worse in crowded areas such as the core of NGC 288 in NUV. For the reasons explained above, at the low spatial resolution of *GALEX*, crowding often caused photometry near the cluster center to be unreliable. We therefore exclude stars located within a given cluster-centric distance, for which we felt that reliable magnitudes could not be obtained on the basis of PSF-fitting photometry. The threshold cluster-centric distance varies from cluster to cluster depending on the density of UV sources. Moreover, because crowding was far more severe in the NUV than in the FUV, we usually adopted different cluster-centric distance thresholds for the two bands.

Finally, we point out that the outer ∼5′ annulus of *GALEX* images is affected by optical distortions that may cause false detections and large magnitude errors (see, e.g., Rey et al. 2007). We note that our photometry is not affected by these problems, because typically this area is well beyond the tidal radii of the clusters in our sample, except for the cases of 47 Tuc and M 3 (NGC 104 and 5272, respectively). For these two clusters, all photometry within the outer ∼5′ annulus was discarded.

Cross-correlation of the FUV and NUV catalogs was performed using CataXcorr, developed at the Observatory of Bologna (P. Montegriffo et al. 2003, private communication), which has the important advantage of allowing a visual check of the quality of the geometric roto-translation solution. The final catalogs consist of stars detected in at least one of the two filters. This choice has been made in order to maximize the number of sources for possible cross-match with optical catalogs. For the reasons explained above, there is a large number of NUV sources without an FUV counterpart. On the other hand, because crowding is more severe in the NUV than in the FUV, there is a (small) number of central FUV sources without reliable NUV magnitudes.

For the reasons discussed above, the depth achievable in *GALEX* CMDs is set by the shallower FUV photometry. In fact, we showed in previous works (e.g., Lanzoni et al. 2007; Dalessandro et al. 2009) that our NUV images are often deep enough to detect stars ∼1 mag fainter than the main-sequence turnoff. With the aim of maximizing the number of stars with magnitude measurements in both *GALEX* bands, we attempted to use the `allframe` routine (Stetson et al. 1989) in order to "force-find" stars in the FUV images on the basis of their positions in the NUV. Results of this experiment are shown in Figure 9. The left panel shows the CMD from photometry based on `allstar`, and on the right panel the CMD obtained from forcing `allframe` to find FUV stars at their known NUV positions is shown. These plots suggest that this use of `allframe` leads to detection of sources 3–4 mag fainter in FUV than just using `allstar`. However, by performing a visual analysis on the images, it became clear that most of the additional FUV detections were not real. To further verify this result, we performed PSF photometry at random FUV background positions ending up with a CMD that is very similar to the one obtained when force-finding FUV stars (gray points in the right panel of Figure 9). For this reason we decided to adopt only the catalogs obtained by using the `allstar` routine as already described. Figure 9 shows also that the two approaches give virtually identical results when stars with $\sigma_{\mathrm{FUV}} > 0.25$ are removed from the CMD.

Photometric depth varies from cluster to cluster according to exposure times (see Table 1), thus being in all cases deeper in the NUV than in the FUV. In our deepest images, we reach FUV ∼ 24.4 and NUV ∼ 25.0. NGC 2419 is the only cluster in our sample (with both FUV and NUV images available) for which it has not been possible to obtain reliable photometry of individual stars. Since NGC 2419 is a cluster with a large population of emitters both at NUV and FUV wavelengths and it is one of the most distant clusters in the Galaxy (d = 87 kpc; Dalessandro et al. 2008), it appears extremely dense in *GALEX* images making photometric measurements of individual stars virtually impossible at the *GALEX* spatial resolution.

[11] See http://www.galex.caltech.edu/researcher/techdoc-ch5.html

Table 1
Target List

Cluster	FUV t_{exp} (s)	NUV t_{exp} (s)	R.A.$_C$ (deg)	Decl.$_C$ (deg)	OBS Date	Cycle
NGC 104	2235	4069	6.085	−72.132	2006 Jul 6	GI1
NGC 288	1606	1606	13.418	−26.245	2004 Dec 6	GI1/MIS
NGC 362	2623	3027	15.809	−70.848	2005 Oct 23	GI1
NGC 1261	1225	1225	48.064	−55.217	2004 Dec 9	GI1
NGC 1851	2797	4487	78.526	−40.047	2004 Dec 10	GI1
NGC 1904	1326	3176	81.196	−24.461	2004 Dec 14	GI1
NGC 2298	10757	22171	102.066	−35.945	2004 Dec 15	GI1
NGC 2808	987	988	137.896	−64.913	2007 Mar 11	GI3
NGC 2419	1262	3695	114.688	38.869	2008 Dec 16	GI4
NGC 4147	1678	1678	182.526	18.542	2006 Mar 29	GI1
NGC 4590	1634	5081	190.020	−26.605	2007 Mar 30	GI1
NGC 5024	1656	1656	198.230	18.169	2007 May 2	GI1
NGC 5053	1781	1782	199.112	17.698	2007 May 3	GI1
NGC 5272	1679	1680	205.547	28.375	2007 May 1	GI1
NGC 5466	1841	3532	211.364	28.535	2007 May 1	GI1
NGC 5897	1590	2936	229.352	−21.010	2007 May 6	GI1
NGC 5904	1563	1566	229.592	2.069	2007 May 12	GI3
NGC 5986	4224	4225	236.514	−37.786	2007 Jun 6	GI3
NGC 6101	2010	2010	247.039	−72.502	2008 Jul 26	GI1
NGC 6218	120	23891	251.811	−1.948	2006 Jul 2	GI1
NGC 6229	1603	5419	251.769	47.477	2007 Apr 13	GI1
NGC 6235	1875	25131	253.373	−22.585	2005 Jun 24	GI1
NGC 6254	1911	25362	254.287	−4.099	2005 Jun 23	GI1
NGC 6273	2264	...	255.603	−26.563	2007 Jun 17	GI3
NGC 6284	5767	4225	236.514	−37.786	2007 Jun 6	GI3
NGC 6341	1911	1911	258.884	43.123	2008 May 25	GI4
NGC 6342	3101	3101	260.730	−19.451	2008 May 27	GI4
NGC 6402	5185	5184	264.500	−3.350	2007 Jun 17	GI3
NGC 6356	3369	3369	260.949	−17.642	2008 May 27	GI4
NGC 6397	1584	409	265.574	−53.770	2008 Jul 17	GI4
NGC 6535	1671	1671	270.670	−0.330	2008 May 31	GI4
NGC 6584	4799	4799	274.578	−52.228	2008 Jul 17	GI4
NGC 6809	840	840	294.994	−31.063	2008 Jul 14	GI4
NGC 6864	1882	4817	301.520	−21.921	2005 Aug 6	GI1
NGC 6981	2470	5039	313.366	−12.537	2005 Aug 5	GI1
NGC 7006	1457	4690	315.375	16.185	2006 Aug 12	GI1
NGC 7089	3143	4418	323.372	−0.823	2005 Aug 5	GI1
NGC 7099	2305	2305	325.197	−23.192	2008 Aug 4	GI4
NGC 7492	1697	3302	347.224	−15.639	2005 Aug 26	GI1
Arp 2	4027	4027	292.355	−30.770	2008 Jul 11	GI4
Pal 11	2120	15771	296.428	−7.942	2005 Jun 17	GI1
Pal 12	1510	3401	326.662	−21.251	2006 Aug 1	GI1
IC 4499	4279	4279	225.077	−82.213	2008 Jul 29	GI4
Terzan 8	3084	3084	295.438	−34.000	2008 Jul 12	GI4

2.3. Deviations from Linearity

The *GALEX* detectors present deviations from linearity when count rates exceed ∼1000 counts s^{-1} (see M07). This affects bright source photometry, particularly in the FUV (see below). In order to correct observed magnitudes, M07 compared aperture photometry for a sample of *HST* spectrophotometric standards observed by *GALEX*, with synthetic photometry based on spectrophotometric data from the CALSPEC database.[12] Because our photometry is based on PSF-fitting instead of aperture photometry, we decided to repeat the analysis done by M07, by performing PSF photometry on the *GALEX* archival data for *HST* spectrophotometric standards, in order to assess the impact of deviations from linearity on our magnitudes. We used 13 of the spectrophotometric standards from M07 (see Table 2)

Table 2
Standard Stars Used in the Nonlinearity Tests

Star	FUV	FUV$_{M07}$	FUV$_{predicted}$	NUV	NUV$_{M07}$	NUV$_{predicted}$
GD50	12.74	12.70	11.98	12.82	12.84	12.57
HZ4	14.55	14.58	14.53	14.52	14.56	14.50
HZ2	13.21	13.20	12.86	13.37	13.39	13.25
G191B2B	12.26	11.47	99.99	11.71	11.65	10.17
GD108	12.49	12.52	12.39	13.08	13.19	12.77
HZ21	13.11	12.99	12.55	13.27	13.30	13.13
GD153	12.78	99.99	11.33	12.37	12.36	11.91
HZ43	12.73	12.31	10.75	11.98	11.98	11.36
LTT9491	16.09	16.16	16.09	14.60	14.64	14.58
G93	12.94	99.99	12.14	12.66	12.67	12.39
NGC 7293	12.12	10.03	10.93	12.38	99.99	11.70
LDS749B	15.63	15.66	15.57	14.75	14.78	14.71
BD33	12.87	12.35	10.51	12.75	12.66	10.47

[12] See http://www.stsci.edu/instruments/observatory/cdbs/calspec.html

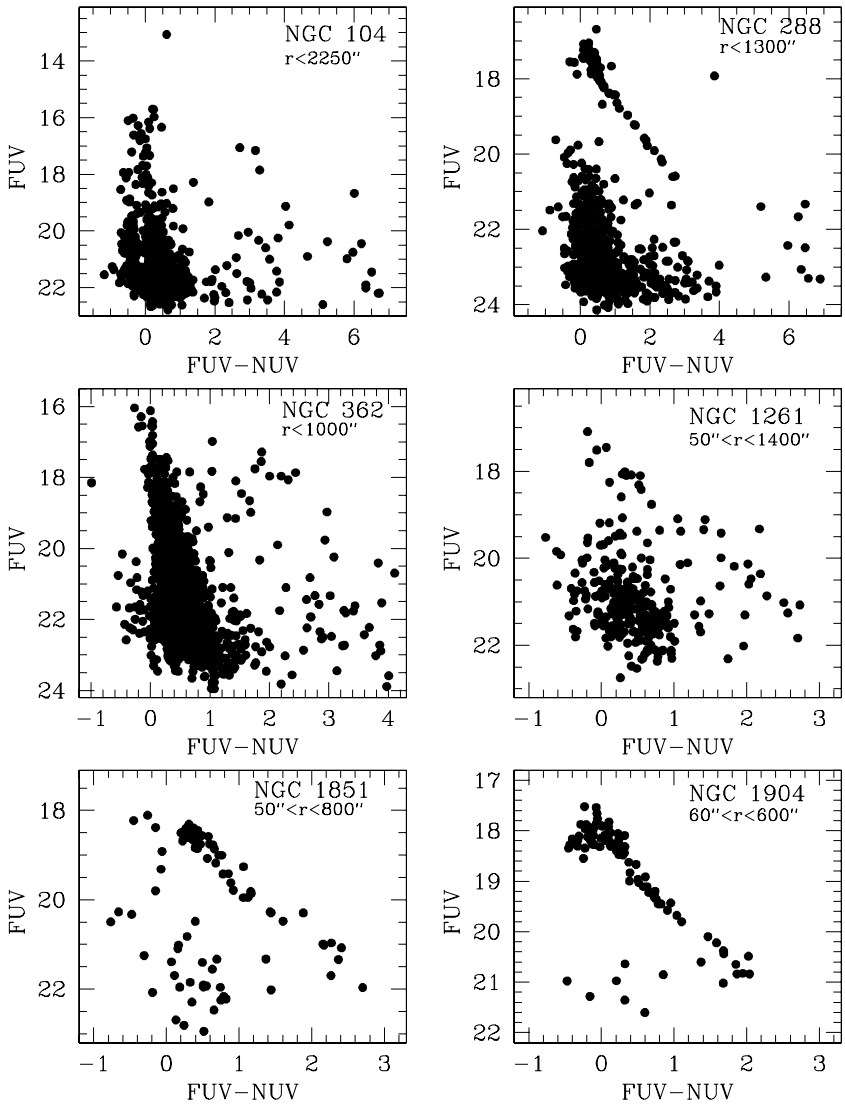

(a)

Figure 11. (a) Color–magnitude diagrams of Galactic GCs. The photometry shown in Figure 11(a) through (g) was *not* corrected for reddening or extinction. Note the variety of HB morphologies. The vast majority of the objects in the CMD of 47 Tuc (NGC 104) and NGC 362 with (FUV_{AB}–NUV_{AB}) $\lesssim$ 1.5 are actually main-sequence stars from the Small Magellanic Cloud.

spanning a range of 4–5 mag both in FUV and NUV. For each of these stars we obtained FUV and NUV magnitudes by using the same procedures described in Section 2.2, and compared our results with those from M07.

The results are displayed in Figure 10, where our measurements are plotted against synthetic magnitudes as reported by M07. Data points for both FUV (filled circles) and NUV (open triangles) are plotted. The solid lines are fits from M07 to the relation between their aperture magnitudes and synthetic photometry, the black (gray) line represents fits to FUV (NUV) data. The dashed line shows the one-to-one relation. It is clear from this figure that nonlinearity becomes detectable in both bands at $\sim 13^{\rm th}$ mag. Deviations increase with increasing brightness, the effect being more severe in the FUV than in the NUV. For the brightest FUV source, nonlinearity leads to a 2.5 mag overestimate in magnitudes, the effect being $\sim$1 mag weaker in the NUV. Most importantly, all but a handful of the stars for which we have photometry are safely below the limit where nonlinearity effects are detectable.

It is interesting to contrast our results with those by M07, by comparing our data points with their fits in Figure 10. In the NUV case, deviations from linearity are consistent between this work and M07, including a star that deviates very strongly from linearity (BD33, in Table 3), for which our photometry is in good agreement with that of M07. On the other hand, the data suggest that nonlinearity effects are slightly stronger in our PSF-fitting photometry than in M07's aperture photometry, particularly in the FUV.

3. THE COLOR–MAGNITUDE DIAGRAMS

The CMDs obtained in this work are displayed in Figures 11(a)–(g). The outstanding variety of colors and magnitudes of UV-bright sources in Galactic GCs is immediately obvious, even on a perfunctory perusal of these diagrams. There are, nonetheless, features that are common to all diagrams, and we briefly comment on those here. In Paper III, we present a new classification of Galactic GCs, based on the morphology of their HBs in UV CMDs, and study correlations between this new HB morphology index with global cluster properties.

We start by discussing the CMD of M 3 (NGC 5272), which is reproduced in better detail in Figure 12. M 3 is a moderately metal-poor Galactic GC ([Fe/H] ~ -1.5) with a relatively blue

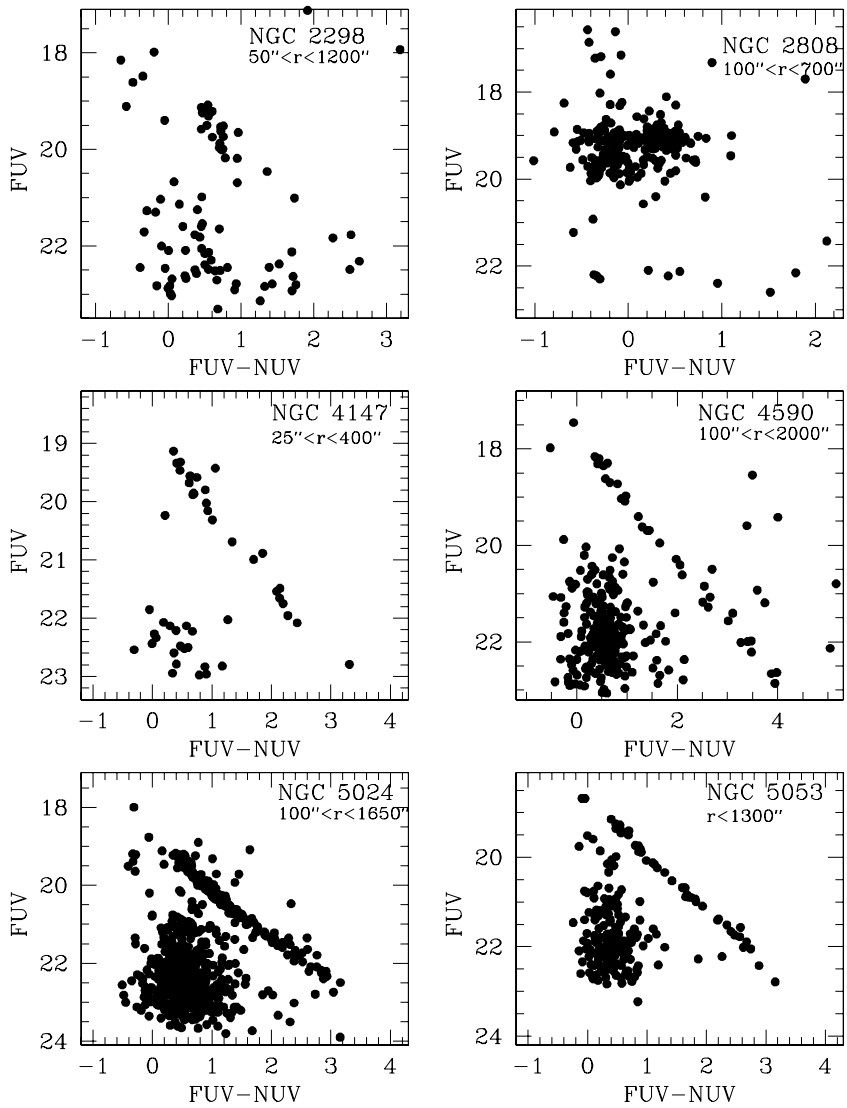

(b)

Figure 11. (Continued). The paucity of sources in the CMD of NGC 2808 is due to the shallowness of the exposures for this cluster.

HB (HB parameter = 0.08; Lee et al. 1994; Borkova & Marsakov 2000). *GALEX* magnitudes were corrected from extinction values estimated using the Cardelli et al. (1989) extinction curve and extinction values from Harris (1996). Extinction in the UV is substantially higher than in the optical, amounting in the case of NGC 5272 to $A_{\rm FUV} \sim 0.08$ and $A_{\rm NUV} \sim 0.09$, as opposed to $A_V \sim 0.03$. We note however, that, because the effective wavelength of the NUV filter coincides with a bump in the Galactic extinction curve (Cardelli et al. 1989), interstellar extinction does not redden FUV–NUV, leading instead to a slight blueing of that color. Finally, absolute magnitudes in Figure 12 were obtained adopting distance moduli taken from Harris (1996).

Only stars located at cluster-centric distances between 120″ and 1300″ are displayed in Figure 12, to minimize crowding effects on photometry performed within the cluster core, and to minimize field contamination beyond the cluster tidal radius. A $T_{\rm eff}$ scale is provided on the top axis of the diagram, which was obtained by interpolating values into (FUV–NUV) versus $T_{\rm eff}$ versus [M/H] tables calculated on the basis of fluxes from Kurucz model atmospheres,[13] adopting the filter responses available on the *GALEX* Web site. Models were adopted for surface gravities typical of HB stars (Dorman et al. 1993), so that the scale does not apply in detail to other stellar types such as blue stragglers and PAGB stars.

The first vacuum-UV CMDs for GCs were obtained by the *Astro*/Ultraviolet Imaging Telescope (e.g., Hill et al. 1992; Parise et al. 1994; Whitney et al. 1994), and the general features of those diagrams are also seen in our *GALEX* photometry. Some of those same features are also seen in *HST* CMDs obtained by Ferraro et al. (1997, 2003). Three main structures are visible in the CMD of this cluster, as indicated in Figure 12. The cluster HB extends from the lower right to the upper left of the diagram, ranging from 4.5 to −0.5 in (FUV–NUV), and from 8 to 2 in $M_{\rm FUV}$. It is obvious from this figure that the "horizontal" branch is not horizontal in the UV (slightly more so in NUV than FUV), and its slope is mainly a result of bolometric correction effects. The HB spans a wide range in $T_{\rm eff}$, going from F stars in the blue HB, at $T_{\rm eff} \sim 7000$ K, all the way to O stars in the so-called extreme HB at $T_{\rm eff} \sim 30{,}000$ K. A few stars are also seen at the blue end of the HB, displaced by up to 1 mag fainter in FUV than the blue tip of the HB, at about $M_{\rm FUV} \sim 3$ and $\rm FUV_{AB}$–$\rm NUV_{AB} \sim -0.25$. Those are the

[13] See http://kurucz.harvard.edu/grids.html

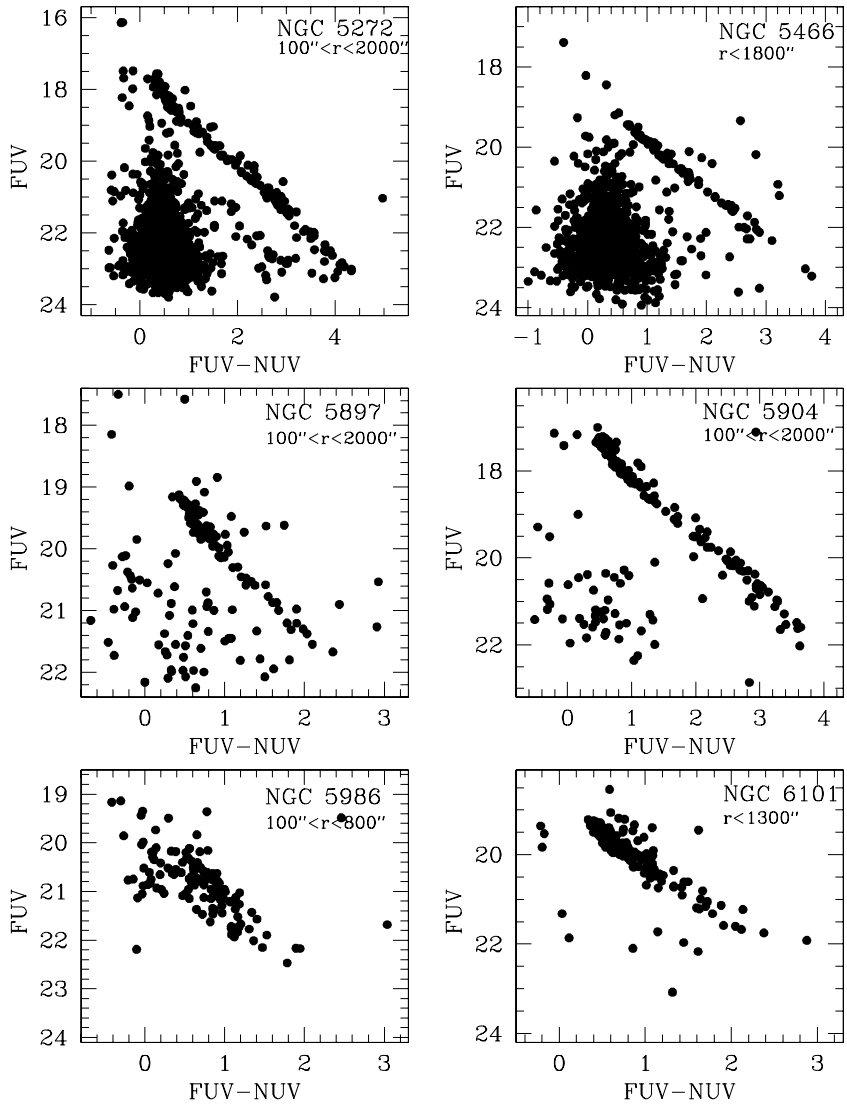

(c)

Figure 11. (Continued)

so-called "Blue Hook" stars, whose origin is still not well understood (e.g., Whitney et al. 1994; Moehler et al. 2004; Busso et al. 2007; Rood et al. 2008; Dalessandro et al. 2011).

A few gaps are apparent along the HB of Figure 12, one of them at (FUV–NUV)/$T_{\rm eff}$ $\sim$ 0.9/8500 K, and two other less prominent ones located at (FUV–NUV)/$T_{\rm eff}$ $\sim$ 3.3/7450 K and 0.0/12,000 K. The latter gap is the one that is the most likely to be real. It corresponds to the "G1" gap, identified by Ferraro et al. (1998) in *HST*/WFPC-2 optical CMDs of M 3 and other Galactic GCs. It also coincides with the position associated with the Grundahl jump—a discontinuity in the HBs of GCs, first pointed out by Grundahl et al. (1998), which manifests itself as a brightening of the Strömgren u or the Johnson U-band magnitudes of stars hotter than $T_{\rm eff}$ $\sim$ 11,500 K. The Grundahl jump has been interpreted by Grundahl et al. (1999) as being due to a decrease of hydrogen opacity relative to metal opacity, associated with an increase of light element opacities due to radiative levitation for $T_{\rm eff}$ $\gtrsim$ 11,500 K. Inspection of Figure 8 of Grundahl et al. (1999) suggests that the differential impact of radiative levitation on FUV- and NUV-like photometric bands can potentially generate a gap with a similar size to that observed in Figure 12. However, a definitive association between this apparent gap and the Grundahl jump depends on currently unavailable synthetic photometry based on detailed model atmosphere calculations for the relevant stellar parameters and abundance patterns.

The remaining two gaps do not seem to have observed counterparts in the CMDs of Ferraro et al. (1998), which casts doubts on the reality of those gaps. As pointed out by Catelan (2008), stochastic effects due to small samples could be to blame, since some of the previously proposed gaps did not stand the test of better quality CMDs, based on more robust samples. According to Catelan (2008), real features such as the Grundahl jump are probably associated with chemical composition discontinuities along the HB, which can manifest themselves through opacity effects due to specific chemical species, which may operate on some photometric bands, but not on others. The latter could conceivably explain the presence of these two gaps in our CMD, but not in those of Ferraro et al. (1998), provided an opacity source can be identified that is important in the NUV/FUV but not in the optical. Alternatively, these gaps may be due to the fact that the nonlinearity of the (FUV–NUV)–$T_{\rm eff}$ relation leads to a color stretching of the redder part of the UV HB, which may make such gaps more

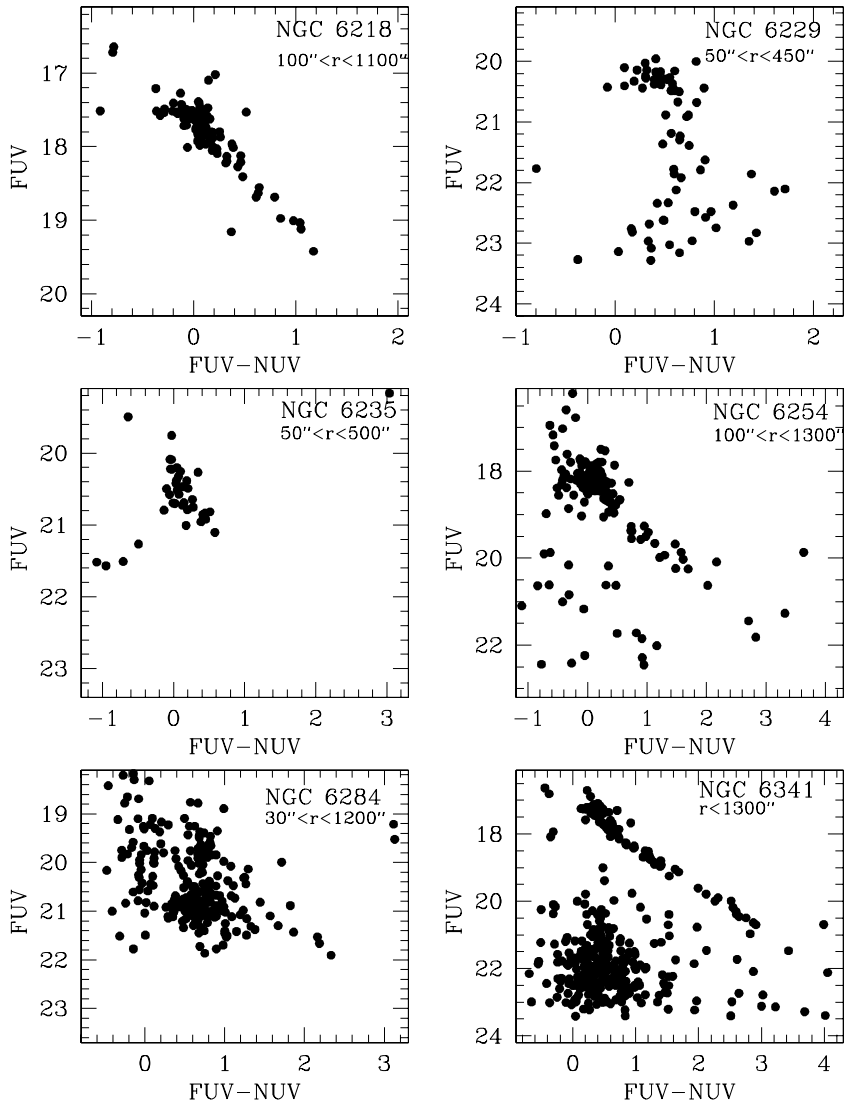

(d)

Figure 11. (Continued)

readily detectable in the UV than in the optical. This issue clearly deserves further investigation in future studies.

Another feature of UV HB morphologies is the clump of stars at $2.5 \lesssim M_{\rm FUV} \lesssim 3.5$ and $0.3 \lesssim$ FUV–NUV $\lesssim 0.8$. This feature is actually an artifact caused by the highly nonlinear character of the color–$T_{\rm eff}$ relation. At (FUV–NUV) ~ 4.0 ($T_{\rm eff} \sim 7000$ K), a 0.5 mag color interval spans a few 100 K in $T_{\rm eff}$, whereas at (FUV–NUV) ~ 0.3 ($T_{\rm eff} \sim 10{,}000$ K) the same color interval spans several 1000 K, leading to the accumulation of data points in that area of the HB for any cluster with a substantial number of stars hotter than $T_{\rm eff} \sim 8500$ K.

The next important population visible in the CMD of Figure 12 is that of blue stragglers. Their identification in this case is easy, as they are spread along a sequence that is parallel, and 1–1.5 mag fainter than the HB (e.g., Ferraro et al. 1999; see also Figure 2 by Ferraro et al. 1997). A Girardi et al. (2000) zero-age main sequence for the metallicity of NGC 5272 is plotted as a dashed line, in order to facilitate the identification of the cluster's blue stragglers. Only the hottest and brightest blue stragglers are detected in the FUV. Lanzoni et al. (2007) and Dalessandro et al. (2009) have recently shown that the combination of *GALEX* data with wide-field optical photometry is a powerful mean to study blue stragglers, and in particular their spatial distribution in GCs.

Another important population in this CMD is that of post-He-core burning stars, whose identification is difficult, given their rarity and the uncertainties surrounding their evolutionary paths in the CMD, as well as their lifetimes. There are two PAGB candidates in this CMD, which are approximately 1.5 mag brighter than the brightest HB stars, at $T_{\rm eff}$ greater than $\sim$20,000 K. See discussion in Section 4.

The cloud of points that is located toward fainter magnitudes and bluer colors than the HB is mostly populated by background sources, with an average color of (FUV–NUV) ~ 0.5 and $M_{\rm FUV} \gtrsim 5$ (FUV $\gtrsim 19$ in Figures 11(a)–(g)). Some of those objects may actually belong to the cluster populations with bright blue stragglers contributing on the red side and young white dwarfs demarcating the blue envelope. Based on WFPC2 data, Ferraro et al. (2001) argued for the presence of young white dwarfs, with ages $\lesssim$13 million years, in the corresponding locus of the (m_{F218W}–m_{F439W}) CMD of 47 Tuc. In particular, they showed that the blue envelope of that CMD population is consistent with theoretical expectations both for the colors and number counts of young white dwarfs. However, while

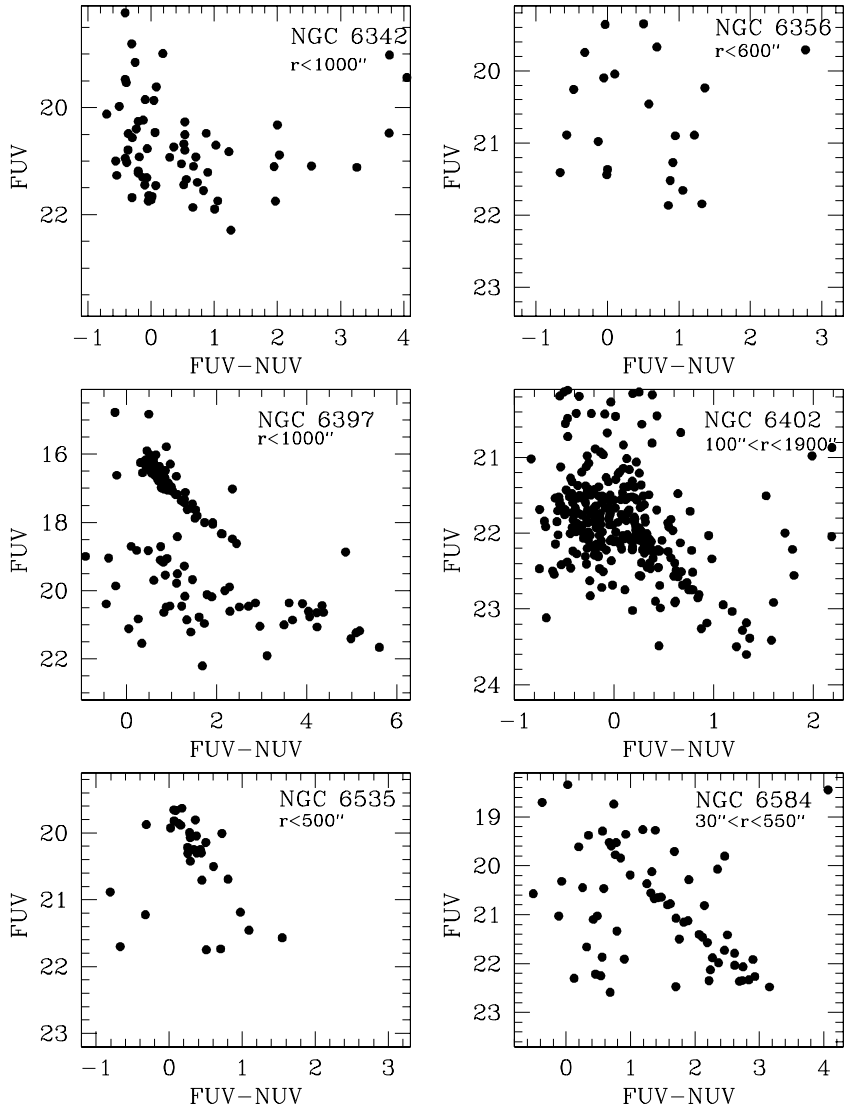

(e)

Figure 11. (Continued)

that study refers to a small region at the center of the cluster, where the background field contamination is expected to be low, the *GALEX* FOV is expected to be heavily contaminated by background objects. In fact, inspection of high-resolution images taken with the wide-field imager, attached to the ESO 2.2 m telescope (Lanzoni et al. 2007), indicated that the majority of the sources in that region of the CMD consists of distant galaxies. In addition, the number of objects in this region of the UV CMD of M 3 is consistent with the number of extragalactic known objects as found in the NASA Extragalactic Database.[14] In summary, the low resolution of *GALEX* images and the relatively low resolution of the ESO 2.2 m images do not allow one to distinguish unequivocally between white dwarfs and blue stragglers on one side, and background galaxies on the other. Therefore, we decide to leave them in the plots, with the caveat that absolute magnitudes should be disregarded for most objects in that region of this diagram.

The effect of crowding on the *GALEX* CMDs can be assessed in Figure 13, where stars in the field of NGC 7089 are plotted. Stars within 2′ from the cluster center are shown as gray triangles, whereas stars at larger cluster-centric distances, within the cluster tidal radius, are plotted with open circles. The different CMD loci occupied by stars within and outside the 2′ radius shows that crowding produces a population of stars artificially brighter and redder than the cluster's HB population. While the brighter magnitudes are a straightforward effect of blending, the apparent redder colors are due to the fact that blending is more severe in the NUV than in the FUV. The case of NGC 7089 is somewhat extreme, since the HB of this cluster is so populous that crowding is important in both FUV and NUV images (Figure 6). In most cases, crowding in the FUV is far less severe, and its effect on CMDs is that of producing a predominantly redder population, due to crowding in the NUV. We also point out that because the "brightening" effect associated with stellar blending should be typically of the order of 0.75 mag, it is possible that some of the very bright stars at FUV $\lesssim$ 14.5 in NGC 7089 may be real UV-bright cluster members. See discussion in Section 4.

4. UV-BRIGHT STARS

While the integrated light of old stellar populations in the FUV is dominated by EHB stars, post-He-core burning stars

[14] http://nedwww.ipac.caltech.edu/

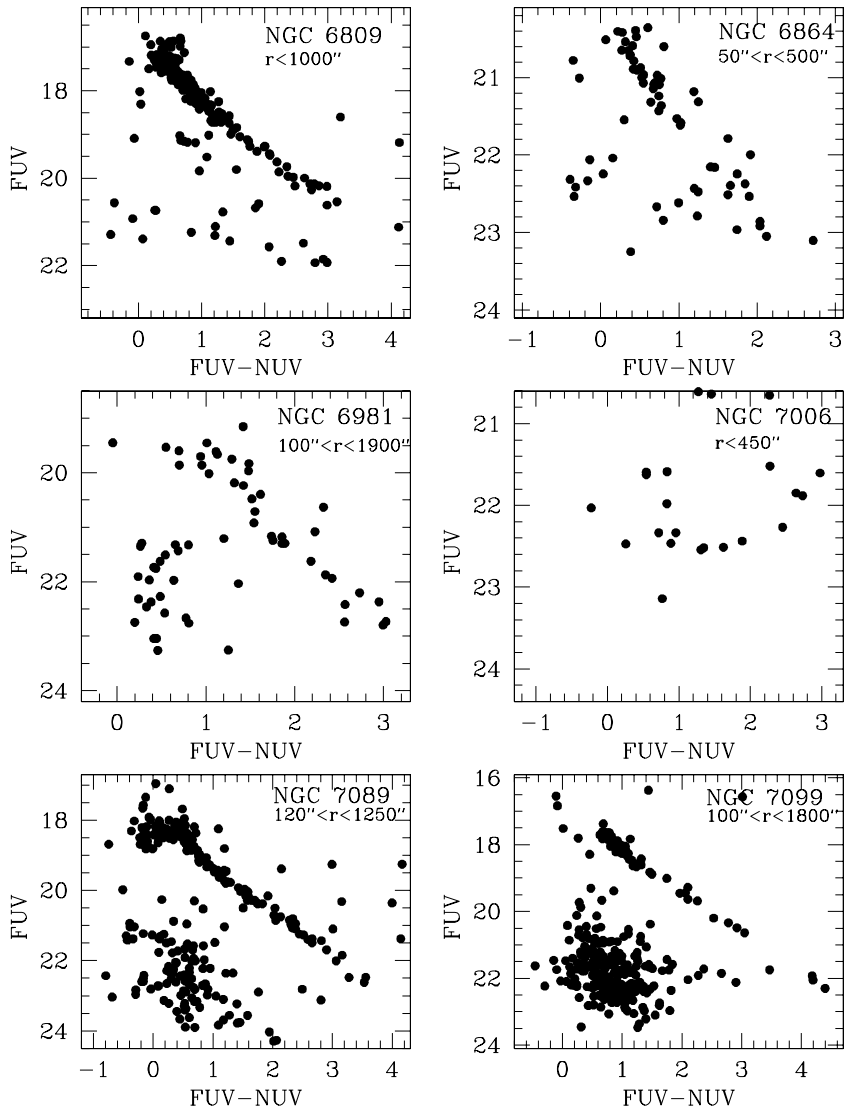

(f)

Figure 11. (Continued)

also contribute a fraction of that radiation (e.g., Greggio & Renzini 1990, 1999; O'Connell 1999). A few definitions are required at this point. According to standard stellar evolution theory, post-HB evolution depends strongly on the mass of the stellar envelope. After core-He exhaustion, stars with the highest envelope masses evolve into the AGB phase, undergoing thermal pulses and eventually losing their envelopes, evolving toward higher temperatures at constant high luminosity as PAGB stars. Stars with lower envelope mass experience a much shier excursion into the AGB phase and never undergo thermal pulses, evolving toward higher temperatures, after envelope loss, at constant, but lower, luminosities. The latter are called post early-AGB (PEAGB) stars. Finally, at the extreme low end of envelope mass, stars never make it to AGB phase after core-He exhaustion, departing the blue end of the HB in a small excursion toward higher luminosities, but never becoming as bright as PEAGB stars. The latter are the so-called AGB-manqué (AGBM) stars.

Our knowledge of the total contribution of these stars to the integrated light of old stellar populations is limited by uncertainties in evolutionary tracks, which are to a large extent due to difficulties in the modeling of mass loss during the AGB phase (van Winckel 2003). GCs are the one type of stellar system where the initial masses of these stars are best constrained, so that observations of post-core-He burning stars in clusters can in principle contribute to the betterment of stellar evolution models. However, stellar evolution proceeds at a very fast pace after the core-He burning stage, with timescales varying between 10^4 and 10^6 yr. The incidence of these stars in stellar systems of relatively low mass, such as GCs, is therefore low, and thus strongly affected by stochastic effects. The wide FOV of *GALEX* and the size of our sample configure an ideal situation for the cataloging of these rare stellar types. We describe in this section the procedure we followed in order to identify PAGB and other UV-bright star candidates.

The paucity of post-core-He burning stars makes their identification solely on the basis of photometry in any given single GC extremely uncertain, though an early attempt was made using a UV CMD of NGC 6752 by Landsman et al. (1996). Because the average number of PAGB stars per cluster is of the order of ∼1, they form no *sequence* in any of the CMDs shown in the previous section. In the absence of a sequence, distinguishing post-core-He burning stars from fore/background field contaminants in the CMD of any individual cluster is very

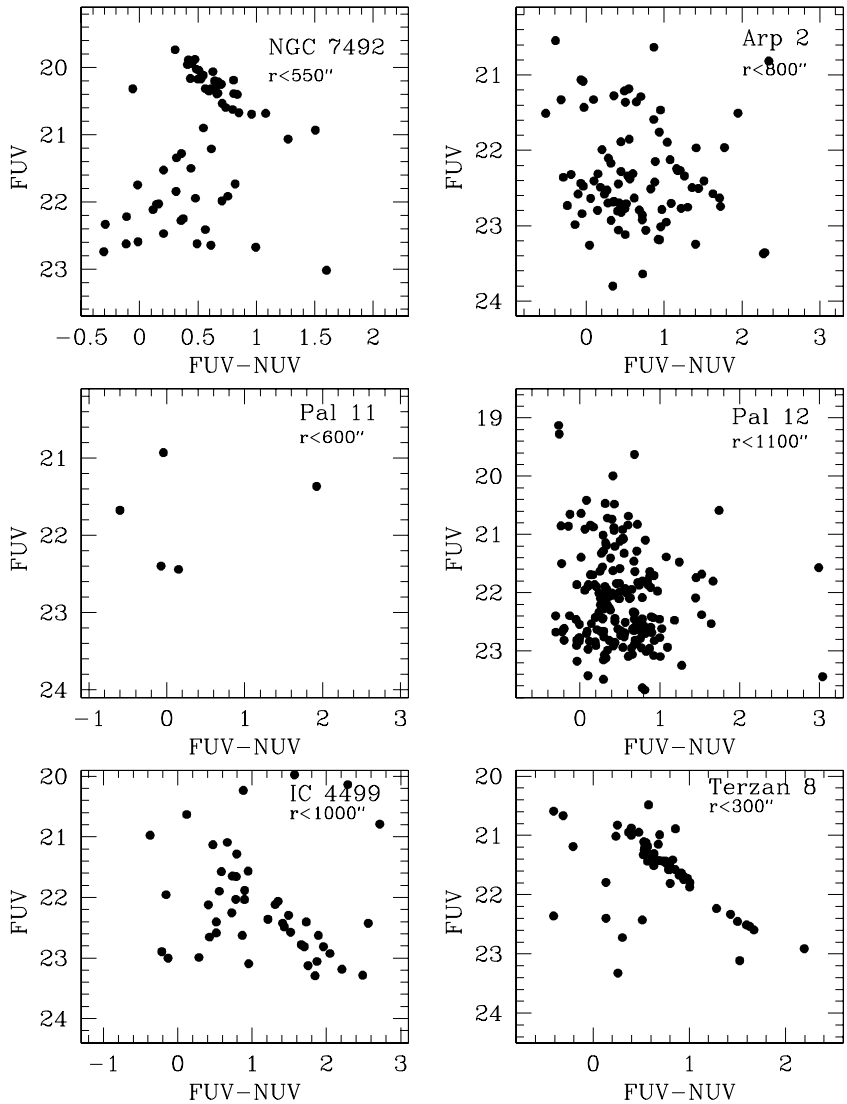

(g)

Figure 11. (Continued)

hard, and usually requires a spectroscopic follow-up. However, stacking the CMDs of many clusters should boost the number of UV-bright stars per unit CMD area, highlighting the locus occupied by stars in these evolutionary stages. Figure 14 shows a stack of the best 23 CMDs from Figures 11(a)–(g), which do not have a very strong background contamination. The clusters included are NGC 1851, 1904, 2298, 4147, 4590, 5024, 5053, 5272, 5466, 5897, 5904, 6101, 6218, 6229, 6254, 6341, 6535, 6584, 6809, 6981, 7089, 7099, and 7492. Data for each cluster were placed on an absolute magnitude scale, adopting reddening and distance modulus from the latest version of the Harris (1996) catalog, and only stars within the radial limits displayed in Figures 11(a)–(g) are shown in Figure 14. The spread in magnitude of the stacked HB is likely caused by uncertainties in the adopted distance moduli and in the adopted reddening values.

Because all the clusters are brought to the same distance, all the typical features of the UV CMDs of old stellar populations appear in sharp contrast in this CMD stack. For instance, the blue straggler sequence stretching below the red part of the HB, and the supra-HB stars in the other extreme of the HB are more clearly seen in the CMD stack than in most individual CMDs of Figures 11(a)–(g). Two stellar sequences brighter than the HB are also apparent in Figure 14. The bluest and brightest in FUV have colors roughly between (FUV–NUV) $= -0.5$ and +0.5, and extend to magnitudes as bright as $M_{\rm FUV} \sim -3$. The other family of stars is located toward redder colors and fainter magnitudes, consisting of a population of stars on average 2–3 mag brighter than the HB, with (FUV–NUV) $\gtrsim$1.5. These stars are mostly foreground contaminants, as discussed below. Finally, we note that there is a population of stars that are brighter than the HB by no more than 1 mag, spread through its entire extension. These are most likely unresolved stellar blends.

We first turn our attention to the main objects of interest, the population of stars revealed by the CMD stack just above the extreme HB stars at $T_{\rm eff}$ of a few tens of 10^4 K. This stellar sequence is too blue and extends toward too bright magnitudes to harbor a significant fraction of blends. We note that in Figure 13 almost all the stars considered to be due to blends produced by crowding effects are redder than (FUV–NUV) $\sim$ 0. Moreover, because Figure 14 excludes stars within central cluster regions, crowding effects should be minimal anyway. So, we conclude that this sequence of hot UV-bright stars constitutes a real population of UV-bright stars hosted by our sample of Galactic GCs. In fact, these stars indeed occupy the same locus

Table 3
Post-He-core Burning Candidates

Star ID	FUV	NUV	R.A.	Decl.	Class
NGC 104-1	13.069	12.448	00:23:58.0	−72:05:30	P(E)AGB
NGC 288-5695	16.687	16.227	12:52:40.9	+26:33:53	AGBM
NGC 362-1625	14.038	14.885	1:03:11.5	−70:49:13	AGBM
NGC 362-372	13.649	14.496	1:02:16.2	−70:51:42	AGBM
NGC 362-1626	13.772	14.632	1:03:38.8	−70:49:12	AGBM
NGC 362-1444	13.769	14.791	1:01:53.1	−70:54:11	AGBM
NGC 362-2413	13.262	14.412	1:03:12.2	−70:59:39	AGBM
NGC 1261-1	14.670	15.483	3:11:48.6	−55:32:36	AGBM
NGC 1261-43	14.734	15.678	3:12:27.8	−55:34:59	AGBM
NGC 1261-8	14.307	15.376	3:11:56.2	−55:17:44	AGBM
NGC 1261-19	15.020	16.067	3:12:10.1	−55:12:22	AGBM
NGC 1851-44	10.895	12.355	05:14:08.6	−40:03:03	P(E)AGB
NGC 2808-17	14.802	14.902	09:12:03.9	−64:51:31	P(E)AGB
NGC 2808-69	15.824	15.874	09:12:02.1	−64:52:36	P(E)AGB
NGC 2808-72	16.187	15.900	09:12:05.7	−64:51:56	P(E)AGB
NGC 2808-84	16.295	16.026	09:12:07.2	−64:51:37	P(E)AGB
NGC 2808-99	15.778	16.163	09:12:11.9	−64:50:37	P(E)AGB
NGC 2808-103	16.178	16.193	09:12:05.4	−64:52:37	P(E)AGB
NGC 2808-118	16.009	16.342	09:11:51.5	−64:51:49	P(E)AGB
NGC 2808-119	16.235	16.344	09:12:06.1	−64:50:35	P(E)AGB
NGC 2808-128	16.714	16.410	09:12:00.5	−64:51:26	P(E)AGB
NGC 2808-132	16.404	16.424	09:12:06.5	−64:52:00	P(E)AGB
NGC 2808-157	17.053	16.614	09:12:00.5	−64:52:12	P(E)AGB
NGC 2808-173	16.614	16.753	9:12:01.7	−64:47:34	AGBM
NGC 2808-206	16.569	17.004	9:11:43.1	−64:52:29	AGBM
NGC 2808-254	17.152	17.229	9:12:22.1	−64:52:38	AGBM
NGC 2808-267	16.859	17.279	9:11:59.9	−64:53:26	AGBM
NGC 2808-314	17.185	17.477	9:12:25.4	−64:52:05	AGBM
NGC 2808-350	17.222	17.577	9:11:41.9	−64:42:06	AGBM
NGC 2808-387	18.110	17.702	9:12:05.3	−64:53:25	AGBM
NGC 2808-421	17.591	17.783	9:12:20.0	−64:50:55	AGBM
NGC 2808-594	18.439	18.216	9:12:05.5	−64:53:47	AGBM
NGC 2808-656	18.240	18.307	9:12:10.8	−64:50:02	AGBM
NGC 2808-670	18.024	18.328	9:11:24.9	−64:52:45	AGBM
NGC 2808-711	18.314	18.406	9:12:12.0	−64:53:15	AGBM
NGC 2808-756	18.288	18.482	9:11:50.9	−64:50:30	AGBM
NGC 2808-1146	18.255	18.944	9:12:17.2	−64:48:04	AGBM
NGC 4590-9	15.925	15.627	12:38:33.0	−26:41:15	AGBM
NGC 5024-5	15.269	15.655	13:14:00.1	+18:31:31	P(E)AGB
NGC 5024-7	15.506	15.832	13:13:10.6	+18:07:36	P(E)AGB
NGC 5024-161	17.994	18.307	13:12:39.5	+18:04:54	AGBM
NGC 5272-2	13.613	13.778	13:42:16.9	+28:26:02	P(E)AGB
NGC 5272-32	16.137	16.488	13:42:01.2	+28:23:25	AGBM
NGC 5272-38	16.146	16.527	13:42:05.9	+28:19:05	AGBM
NGC 5466-1	13.075	13.997	14:03:17.2	+28:39:30	PAGB
NGC 5466-36	17.391	17.793	14:05:31.6	+28:33:10	AGBM
NGC 5897-26	16.564	16.719	15:18:56.6	−21:08:40	AGBM
NGC 5897-34	17.578	17.080	15:17:23.7	−20:37:56	AGBM
NGC 5897-50	17.308	17.648	15:18:04.7	−20:47:02	AGBM
NGC 5897-61	17.499	17.835	15:18:40.6	−21:16:08	AGBM
NGC 5904-1	13.318	13.361	15:18:34.2	+02:05:02	P(E)AGB
NGC 5904-3	14.413	14.612	15:18:32.8	+01:54:54	AGBM
NGC 5986-634	19.140	19.443	15:46:38.1	−37:41:25	AGBM
NGC 5986-701	19.165	19.580	15:46:46.5	−37:49:38.	AGBM
NGC 6101-4874	16.782	17.159	16:26:47.1	−72:15:24	AGBM
NGC 6218-48	16.643	17.423	16:47:12.6	−01:41:24	AGBM
NGC 6235-154	18.585	19.174	16:53:39.1	−22:16:17	AGBM
NGC 6235-184	19.449	19.412	16:52:47.4	−22:04:14	AGBM
NGC 6235-186	19.578	19.437	16:52:51.1	−22:14:21	AGBM
NGC 6235-196	18.847	19.507	16:52:49.4	−22:11:50	AGBM
NGC 6235-254	19.754	19.780	16:53:18.0	−22:11:39	AGBM
NGC 6235-355	19.496	20.136	16:53:43.4	−22:17:36	AGBM
NGC 6235-439	19.734	20.350	16:53:38.3	−22:01:02	AGBM
NGC 6235-43	16.919	17.475	16:53:20.8	−22:02:40	P(E)AGB
NGC 6254-66	14.244	15.544	16:56:48.0	−04:04:33	AGBM
NGC 6254-112	13.813	15.052	16:57:02.8	−04:08:19	AGBM

Table 3
(Continued)

Star ID	FUV	NUV	R.A.	Decl.	Class
NGC 6254-117	13.990	15.071	16:57:05.2	−04:07:56	AGBM
NGC 6254-152	13.208	14.829	16:56:43.7	−04:05:41	AGBM
NGC 6254-189	14.390	15.851	16:57:06.3	−04:03:19	AGBM
NGC 6254-241	13.433	14.564	16:57:14.7	−04:05:03	AGBM
NGC 6254-242	11.096	12.905	16:57:09.4	−04:04:24	P(E)AGB
NGC 6254-364	14.167	15.680	16:57:01.1	−04:04:30	AGBM
NGC 6284-2	13.175	13.772	17:04:10.4	−24:27:57	P(E)AGB
NGC 6284-85	16.156	16.484	17:04:29.7	−24:29:20	P(E)AGB
NGC 6284-116	17.032	16.921	17:04:45.0	−24:32:60	P(E)AGB
NGC 6284-154	17.282	17.207	17:05:10.8	−24:32:24	P(E)AGB
NGC 6284-212	17.385	17.606	17:03:11.4	−24:51:31	P(E)AGB
NGC 6342-110	18.991	18.803	17:21:38.3	−19:34:04	P(E)AGB
NGC 6356-1	13.089	14.059	17:23:25.2	−17:58:15	P(E)AGB
NGC 6356-311	18.480	18.867	17:23:45.9	−17:41:59	AGBM
NGC 6356-424	18.877	19.243	17:24:04.0	−17:49:37	AGBM
NGC 6356-480	19.357	19.390	17:23:45.6	−17:50:17	AGBM
NGC 6356-849	19.745	20.061	17:23:39.9	−17:43:57	AGBM
NGC 6397-149	14.773	15.029	17:41:30.620	−53:28:18.90	AGBM
NGC 6397-438	14.827	14.330	17:39:44.524	−53:43:29.37	AGBM
NGC 6397-522	13.640	13.680	17:40:38.428	−53:38:32.20	AGBM
NGC 6402-31	17.581	17.508	17:37:33.2	−03:14:52	PAGB
NGC 6402-58	18.079	18.528	17:37:37.3	−03:15:45	P(E)AGB
NGC 6402-92	19.206	19.170	17:37:38.1	−03:14:09	P(E)AGB
NGC 6402-99	19.142	19.261	17:37:33.6	−03:15:27	P(E)AGB
NGC 6402-102	18.669	19.321	17:38:20.1	−03:10:06	P(E)AGB
NGC 6402-142	19.169	19.718	17:37:26.1	−03:14:55	P(E)AGB
NGC 6402-143	19.045	19.718	17:37:28.6	−03:15:17	P(E)AGB
NGC 6402-156	19.663	19.823	17:37:30.9	−03:17:40	P(E)AGB
NGC 6402-160	19.039	19.838	17:36:38.0	−03:23:12	P(E)AGB
NGC 6402-171	19.627	19.900	17:37:37.2	−03:14:60	P(E)AGB
NGC 6402-193	20.046	20.050	17:37:36.4	−03:15:34	P(E)AGB
NGC 6402-202	20.016	20.074	17:37:31.8	−03:15:01	P(E)AGB
NGC 6402-224	20.167	20.144	17:37:40.5	−03:14:58	P(E)AGB
NGC 6864-8	15.853	15.412	20:06:05.5	−21:54:59	PAGB
NGC 6864-52	16.892	17.383	20:05:51.3	−21:42:19	P(E)AGB
NGC 6864-77	18.125	17.832	20:05:19.2	−22:04:21	AGBM
NGC 6864-102	18.669	18.126	20:07:01.8	−21:46:18	AGBM
NGC 6864-212	19.620	19.086	20:04:55.2	−21:51:57	AGBM
NGC 6864-224	19.632	19.138	20:06:40.8	−22:00:23	AGBM
NGC 6864-225	19.631	19.140	20:05:21.5	−21:53:06	AGBM
NGC 6864-452	19.286	20.017	20:06:10.5	−21:38:58	AGBM
NGC 7006-16	16.834	17.385	21:01:35.1	+16:06:10	AGBM
NGC 7089-407	12.492	13.221	21:33:31.4	−00:49:09	P(E)AGB
NGC 7089-387	12.839	17.126	21:33:35.6	−00:51:22	P(E)AGB
NGC 7089-234	14.175	15.013	21:33:19.7	−00:47:5	AGBM
NGC 7089-194	14.788	15.834	21:33:17.9	−00:49:58	AGBM
NGC 7089-765	14.326	14.938	21:32:29.4	−00:48:31	AGBM
NGC 7089-89	14.571	15.579	21:33:30.9	−00:47:20	AGBM
NGC 7099-2	13.449	13.362	21:39:56.7	−23:11:56	P(E)AGB
NGC 7099-10	14.763	15.058	21:40:18.1	−23:13:23	AGBM
NGC 7 099-68	16.545	16.651	21:41:38.7	−22:54:11	AGBM
Arp 2-25	18.227	17.757	19:27:45.3	−30:24:51	P(E)AGB
Arp 2-61	19.555	19.860	19:29:11.2	−30:17:09	AGBM
Arp 2-70	19.831	20.254	19:28:57.0	−30:27:59	AGBM
Pal 12-25	16.423	16.498	21:47:49.2	−21:17:33	AGBM
Pal 12-59	18.094	17.556	21:46:04.3	−21:21:46	AGBM
IC 4499-485	19.811	20.409	14:56:54.2	−82:12:22	AGBM
Ter 8-38	17.800	17.270	19:41:40.8	−34:03:59	P(E)AGB

as the PAGB, PEAGB, and AGBM stars identified by Brown et al. (2008) in a STIS UV CMD of M 32 stars (their Figure 3). In order to gain further insight into their nature, we reproduce the CMD stack in Figure 15, overlaying evolutionary tracks by Brown et al. (2008) for a PEAGB and a PAGB star of ∼0.5

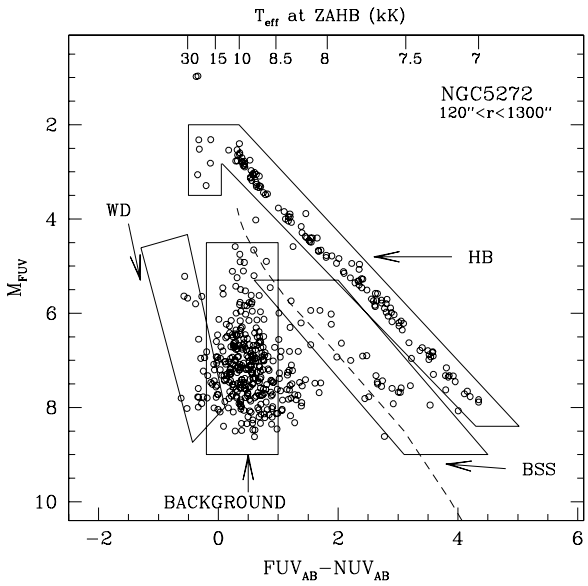

Figure 12. Reddening- and distance modulus-corrected CMD of NGC 5272 (M 3), indicating the main populations that dominate the UV light of old stellar populations. The $T_{\rm eff}$ scale on the top axis was obtained using Kurucz model fluxes (http://kurucz.harvard.edu/grids.html) for the cluster metallicity, adopting surface gravities from Dorman et al. (1993) and is appropriate only for HB stars. Note the presence of gaps in the cluster horizontal branch, and an artificial clump of HB stars around (FUV–NUV) ~ 0.5, which is due to the strongly nonlinear color–$T_{\rm eff}$ relation. The brightest and hottest cluster blue stragglers are clearly detected, 1–1.5 mag below the HB. Two candidate PAGB stars are visible at $M_{\rm FUV} \sim 1$ and (FUV–NUV) ~ -0.5. A few white dwarf candidates are also detected, but, at the *GALEX* resolution, it is very difficult to distinguish them from background sources. The latter are predominantly extragalactic.

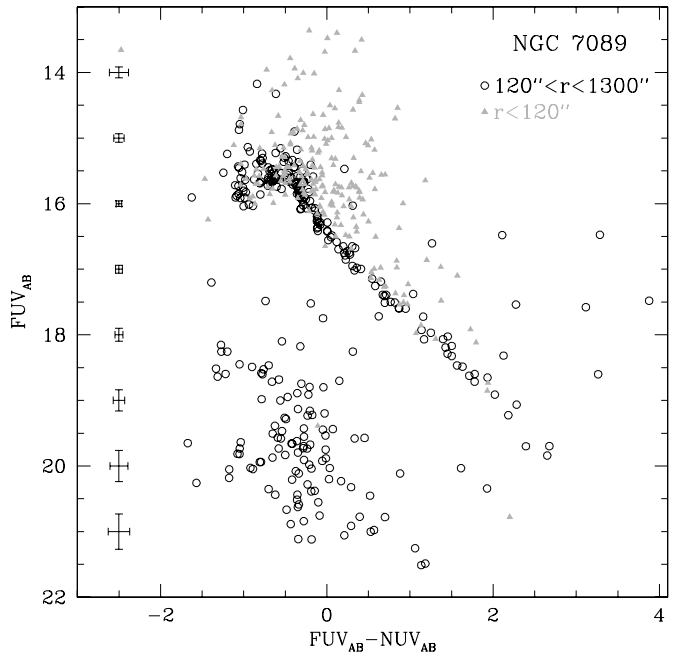

Figure 13. Observed CMD of one of our densest clusters, NGC 7089, illustrating the effect of crowding in our photometry. Gray triangles represent sources within 2′ of the cluster center, and all others are located between that inner radial distance and the cluster tidal radius (1300″). The main effect of crowding is to displace stars toward brighter FUV magnitudes and redder colors. The color effect is due to the fact that crowding is more severe in the NUV than in the FUV.

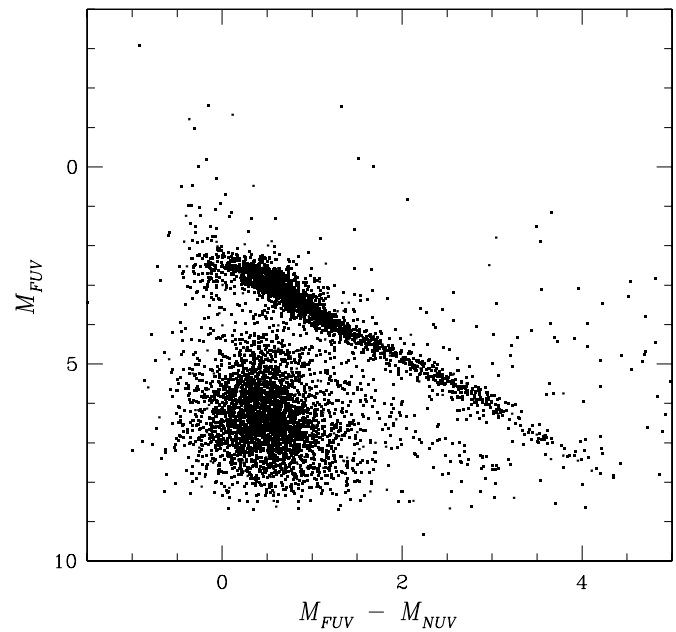

Figure 14. Stacked color–magnitude diagram of 23 Galactic GCs (see Section 4). The UV-bright population composed by candidate post-He-core burning at ($M_{\rm FUV}$–$M_{\rm NUV}$) ~ 0 and $M_{\rm FUV} \lesssim 2$ is clearly seen in this stack. Redder stars brighter than the HB are likely to be predominantly background sources. The blue stragglers can also be very clearly spotted in this diagram, below the redder half of the HB.

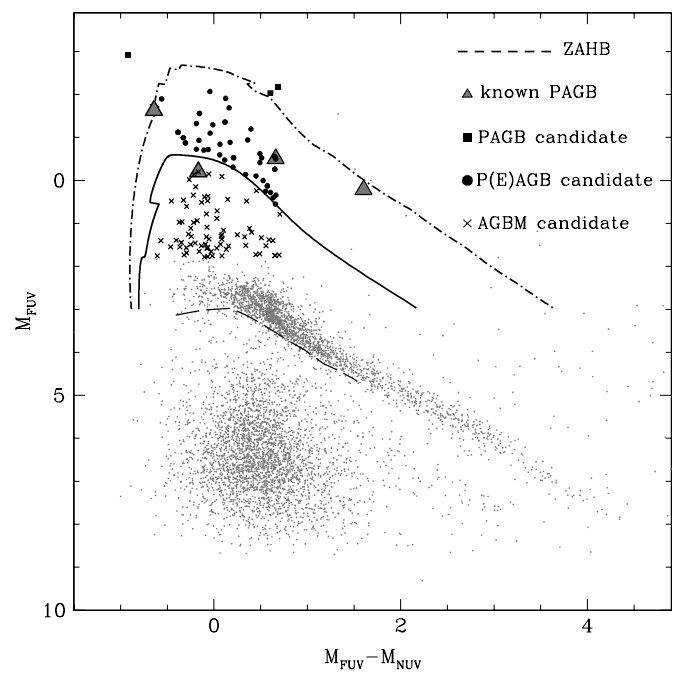

Figure 15. Stacked color–magnitude diagram from Figure 14 (gray dots), with theoretical models from Brown et al. (2008) overlaid on the data. The thick solid line represents the post-HB evolutionary path for a star of $M = 0.77\,M_\odot$, while the dash-dotted line is for an $M = 0.515\,M_\odot$ star. The dashed model is the ZAHB. The solid squares represent candidate PAGB stars. Large circles are candidate P(E)AGBs and crosses are candidate AGBM stars. Large gray triangles indicate the positions of a few well-known PAGB stars. Note that, while for all the other stellar types photometry is only plotted for stars within the cluster-centric limits shown in Figures 11(a)–(g), photometry is shown for all PAGB stars. See discussion in Section 4.

(dash-dotted line) and $0.8\,M_\odot$ (thick solid line), respectively. The model prediction for the zero-age horizontal branch (ZAHB; dashed line) is also shown, which matches very well the lower envelope of our observed HB.

On the basis of the discussion above, we can use the evolutionary tracks in Figure 15 to assign the UV-bright stars in our sample to the above evolutionary classes. Candidates for the different classes are listed in Table 3 and shown in Figure 15, where the data from Figure 14 are shown as gray dots. Filled circles indicate the positions of all PAGB candidates in our entire cluster sample, regardless of their cluster-centric distances. The large gray triangles indicate the positions of a few PAGB stars known to exist in clusters from our sample. We chose not to impose a cluster-centric distance cut in our selection of PAGB and PEAGB candidates, because they are bright enough that crowding effects on their photometry are minimal. That is not the case of AGBM stars, though, which lie close enough in magnitude to the HB that their locus in the CMD may be substantially contaminated by unresolved pairs of HB stars. Therefore, the list of AGBM candidates presented in Table 3 only includes stars within the cluster-centric distance thresholds displayed in Figures 11(a)–(g). We consider stars brighter than the ZAHB by more than 1 mag in $M_{\rm FUV}$ and fainter than the PEAGB tracks to be AGBM candidates. Stars brighter than the PEAGB class are either PEAGB or PAGB candidates, we therefore refer to these stars as P(E)AGB. In view of the uncertainties in evolutionary tracks and the possible contamination of our magnitudes by stellar blends (for stars within the crowded areas of the clusters), we refrain from attempting a distinction between the latter two classes in our sample. Finally, stars brighter than the PAGB track are considered to be PAGB candidates. Note that two of the stars identified as PAGB in previous literature (large gray triangles) would be classified as AGBM and P(E)AGB according to our classification scheme. We also impose a color cut in our definition of PAGB, PEAGB, and AGBM candidates, by requiring that they have (FUV–NUV) < 0.7. Note that the AGBM and P(E)AGB candidates identified in Figure 15 include stars from *all* clusters in our sample, not only the 23 clusters included in the stacked CMD from Figure 14.

Finally, we focus on the redder population of stars brighter than the HB. According to Brown et al. (2008) tracks, PAGB stars spend only 25% of their time with colors redder than $\rm FUV_{AB}$–$\rm NUV_{AB} \sim 0.7$, so the fact that there are more bright stars in Figure 14 on the red side of that color threshold than in the blue side is strongly suggestive of the presence of back/foreground contamination. There are approximately 26 stars in Figure 14 with $M_{\rm FUV} > 2.2$ and $\rm FUV_{AB}$–$\rm NUV_{AB} < 0.7$. Conversely, there are approximately 67 stars with brighter than the HB by ∼1 mag and with $0.7 < \rm FUV_{AB}$–$\rm NUV_{AB} < 5$. If the evolutionary tracks are correct, we would expect to find no more than ∼9 stars in that region of the CMD. Therefore, we suggest that the vast majority of the bright stars redder than $\rm FUV_{AB}$–$\rm NUV_{AB} \sim 0.7$ are not cluster members, likely being foreground A and F stars. That is not to say, of course, that there are no cluster PAGB stars in that region of the diagram—in fact, they are very likely to be there, but finding them on the basis of *GALEX* data alone would be like finding needles in a haystack. Therefore, we impose a color cut in our definition of PAGB, PEAGB, and AGBM candidates, by requiring that they have $\rm FUV_{AB}$–$\rm NUV_{AB} < 0.7$. This color cut is aimed at minimizing contamination of the candidate sample by back/foreground contaminants sources.

5. CONCLUSIONS

We have used *GALEX* to image 44 Galactic GCs in the FUV and NUV, thus creating the largest homogeneous database of the UV properties of these systems. In this paper, we describe the sample selection, observations, and data reduction, presenting a brief description of the main features of the UV CMDs. HB stars are the most important feature of the UV CMDs, and our CMDs reveal an outstanding variety in the shape of the HB in our cluster sample. Blue straggler stars are also detected in many clusters. We present a catalog of PAGB, PEAGB, and AGBM candidates, which should be useful for studies of these rare, but UV-bright, stellar types. We hope these data will provide better constraints on models of stellar evolution during, and after, the HB phase. In Paper II, we present the integrated UV photometry for this sample, while a new classification scheme of the morphology of the HBs of Galactic GCs in UV is presented in Paper III.

GALEX provided us with an opportunity, unique in this decade, to collect precious data that will be crucial to help untangling the intricacies of the latest stages of evolution of low-mass stars, so as to allow a deeper understanding of the UV properties of old stellar populations. We hope that this data set will enable notable progress in this field during the upcoming years. The photometric catalogs can be downloaded from http://www.cosmic-lab.eu.

Based on observations made with the NASA *Galaxy Evolution Explorer*. *GALEX* is operated for NASA by the California Institute of Technology under NASA contract NAS5-98034. We thank Allen Sweigart and Tom Brown for making available the theoretical evolutionary tracks employed in this paper. R.P.S. acknowledges funding by *GALEX* grants NNG05GE50G and NNX08AW42G and support from Gemini Observatory, which is operated by the Association of Universities for Research in Astronomy, Inc., on behalf of the international Gemini partnership of Argentina, Australia, Brazil, Canada, Chile, the United Kingdom, and the United States of America. E.D. thanks the hospitality and support from Gemini Observatory where most of this work was developed, during two extended visits in 2009 and 2010, and a shorter visit in 2011. This research is also part of the project COSMIC-LAB funded by the European Research Council (under contract ERC-2010-AdG-267675). The financial contribution of the Italian Istituto Nazionale di Astrofisica (INAF, under contract PRIN-INAF 2008) and the Agenzia Spaziale Italiana (under contract ASI/INAF/I/009/10) is also acknowledged. S.T.S. and J.R. are partially supported by *GALEX* grant GI3-0075/NNX07AP07G. S.-C.R. acknowledges support from Basic Science Research Program (No. 2009-0070263) and the Center for Galaxy Evolution Research through the National Research Foundation of Korea (NRF). S.-J.Y. acknowledges support from Mid-career Researcher Program (No. 2009-0080851) and Basic Science Research Program (No. 2009-0086824) through the NRF of Korea.

REFERENCES

Borkova, T. V., & Marsakov, V. A. 2000, Astron. Rep., 44, 665
Brown, T. M., Smith, E., Ferguson, H. C., et al. 2008, ApJ, 682, 319
Brown, T. M., Sweigart, A. V., Lanz, T., Landsman, W. B., & Hubeny, I. 2001, ApJ, 562, 638
Busso, G., Cassisi, S., Piotto, G., et al. 2007, A&A, 474, 105
Cardelli, J. A., Clayton, G. C., & Mathis, J. S. 1989, ApJ, 345, 245
Catelan, M. 2008, Mem. Soc. Astron. Ital., 79, 388
Catelan, M. 2009, Ap&SS, 320, 261
Code, A. D. 1969, PASP, 81, 475
Dalessandro, E., Beccari, G., Lanzoni, B., et al. 2009, ApJS, 182, 509
Dalessandro, E., Lanzoni, B., Ferraro, F. R., et al. 2008, ApJ, 681, 311
Dalessandro, E., Salaris, M., Ferraro, F. R., et al. 2011, MNRAS, 410, 694
Dalessandro, E., et al. 2012, AJ, submitted
Dorman, B., O'Connell, R. W., & Rood, R. T. 1995, ApJ, 442, 105

Dorman, B., Rood, R. T., & O'Connell, R. W. 1993, ApJ, 419, 596
Ferraro, F. R., D'Amico, N., Possenti, A., Mignani, R. P., & Paltrinieri, B. 2001, ApJ, 561, 337
Ferraro, F. R., Paltrinieri, B., Fusi Pecci, F., Rood, R. T., & Dorman, B. 1998, ApJ, 500, 311
Ferraro, F. R., Paltrinieri, B., Fusi Pecci, F., et al. 1997, A&A, 324, 915
Ferraro, F. R., Paltrinieri, B., Rood, R. T., & Dorman, B. 1999, ApJ, 522, 983
Ferraro, F. R., Sills, A., Rood, R. T., Paltrinieri, B., & Buonanno, R. 2003, ApJ, 588, 464
Girardi, L., Bressan, A., Bertelli, G., & Chiosi, C. 2000, A&AS, 141, 371
Greggio, L., & Renzini, A. 1990, ApJ, 364, 35
Greggio, L., & Renzini, A. 1999, Mem. Soc. Astron. Ital., 70, 691
Grundahl, F., Catelan, M., Landsman, W. B., Stetson, P. B., & Andersen, M. I. 1999, ApJ, 524, 242
Grundahl, F., Vandenberg, D. A., & Andersen, M. I. 1998, ApJ, 500, L179
Harris, W. E. 1996, AJ, 112, 1487
Hill, R. S., Hill, J. K., Landsman, W. B., et al. 1992, ApJ, 395, L17
Landsman, W. B., Sweigart, A. V., Bohlin, R. C., et al. 1996, ApJ, 472, L93
Lanzoni, B., Sanna, N., Ferraro, F. R., et al. 2007, ApJ, 663, 1040
Law, D. R., & Majewski, S. R. 2010, ApJ, 718, 1128
Lee, Y.-W., Demarque, P., & Zinn, R. 1994, ApJ, 423, 248
Lee, Y.-W., Joo, S.-J., Han, S.-I., et al. 2005, ApJ, 621, L57
Moehler, S. 2001, PASP, 113, 162
Moehler, S., Sweigart, A. V., Landsman, W. B., Hammer, N. J., & Dreizler, S. 2004, A&A, 415, 313
Morrissey, P., Conrow, T., Barlow, T. A., et al. 2007, ApJS, 173, 682
Morrissey, P., Schiminovich, D., Barlow, T. A., et al. 2005, ApJ, 619, L7
O'Connell, R. W. 1999, ARA&A, 37, 603
O'Connell, R. W., Dorman, B., Shah, R. Y., et al. 1997, AJ, 114, 1982
Parise, R. A., Maran, S. P., Landsman, W. B., et al. 1994, ApJ, 423, 305
Rey, S.-C., Rich, R. M., Sohn, S. T., et al. 2007, ApJS, 173, 643
Rey, S.-C., Sohn, S. T., Beasley, M. A., et al. 2009, ApJ, 700, L11
Rood, R. T., Beccari, G., Lanzoni, B., et al. 2008, Mem. Soc. Astron. Ital., 79, 383
Schiavon, R. P. 2007, ApJS, 171, 146
Sohn, S. T., O'Connell, R. W., Kundu, A., et al. 2006, AJ, 131, 866
Stetson, P. B. 1987, PASP, 99, 191
Stetson, P. B., Hesser, J. E., Smith, G. H., Vandenberg, D. A., & Bolte, M. 1989, AJ, 97, 1360
Trager, S. C., Worthey, G., Faber, S. M., & Dressler, A. 2005, MNRAS, 362, 2
van Winckel, H. 2003, ARA&A, 41, 391
Whitney, J. H., O'Connell, R. W., Rood, R. T., et al. 1994, AJ, 108, 1350